ANNUAL REVIEWS

Kinetics of Drug Binding and Residence Time

Mattia Bernetti,[1] Matteo Masetti,[1] Walter Rocchia,[2] and Andrea Cavalli[1,3]

[1]Department of Pharmacy and Biotechnology, University of Bologna, I-40126 Bologna, Italy

[2]CONCEPT Laboratory, Istituto Italiano di Tecnologia, I-16163 Genova, Italy;
email: walter.rocchia@iit.it

[3]Computational Sciences Domain, Istituto Italiano di Tecnologia, I-16163 Genova, Italy;
email: andrea.cavalli@iit.it

ANNUAL REVIEWS CONNECT

www.annualreviews.org

- Download figures
- Navigate cited references
- Keyword search
- Explore related articles
- Share via email or social media

Keywords

binding kinetics, transition state theory, drug discovery, molecular dynamics, Brownian dynamics, surface plasmon resonance

Abstract

The kinetics of drug binding and unbinding is assuming an increasingly crucial role in the long, costly process of bringing a new medicine to patients. For example, the time a drug spends in contact with its biological target is known as residence time (the inverse of the kinetic constant of the drug-target unbinding, $1/k_{off}$). Recent reports suggest that residence time could predict drug efficacy in vivo, perhaps even more effectively than conventional thermodynamic parameters (free energy, enthalpy, entropy). There are many experimental and computational methods for predicting drug-target residence time at an early stage of drug discovery programs. Here, we review and discuss the methodological approaches to estimating drug binding kinetics and residence time. We first introduce the theoretical background of drug binding kinetics from a physicochemical standpoint. We then analyze the recent literature in the field, starting from the experimental methodologies and applications thereof and moving to theoretical and computational approaches to the kinetics of drug binding and unbinding. We acknowledge the central role of molecular dynamics and related methods, which comprise a great number of the computational methods and applications reviewed here. However, we also consider kinetic Monte Carlo. We conclude with the outlook that drug (un)binding kinetics may soon become a go/no go step in the discovery and development of new medicines.

1. INTRODUCTION

In chemistry, kinetics is the study of the rates of chemical reactions. It deals with the quantitative description of how fast a chemical reaction occurs. Chemical kinetics aims to identify the factors affecting these rates and understand the key aspects of reaction pathways. Reactions and associated kinetics can occur through single-step mechanisms or very complex multistep mechanisms, which may take place in biological systems. For instance, multistep chemical mechanisms can usually be observed in enzymatic reactions. Kinetic studies in this context aim to evaluate the rates of variation of substrate concentration and determine the rates that are constant for all the steps.

Recently, kinetics has gained the interest of the drug discovery community due to reports that it is possible to predict the efficacy of a new drug in vivo and in humans by measuring the unbinding kinetics (1–4). From a mechanistic standpoint, the process of a drug binding to its biological target may be considered a multistep reaction mechanism. The eventual on and off rates (macroscopic k_{on} and k_{off}, respectively; see **Figure 1**) may be influenced by microscopic rate constants associated with binding and unbinding, target protein conformational changes and/or isomerization, and so on. In particular, the overall duration of a receptor-ligand complex will be influenced by both the rate of ligand association (k_{on}) and the rate of binary complex dissociation (k_{off}). The time a drug spends in contact with its biological target (usually referred to as the residence time, i.e., $1/k_{off}$) is now considered a key parameter for optimization because there is some evidence that it can predict drug efficacy in vivo (2, 5–8).

Here, we consider the kinetics of drug binding and unbinding, focusing on residence time determination and computational prediction because of its increasingly large role in drug discovery programs (2, 6, 9). We first describe the theoretical background of kinetics in chemical reactions from a classical physicochemical standpoint. We then briefly review the main experimental techniques used to determine the (un)binding kinetics, and their key applications. We then discuss the many recent computational approaches to estimating and predicting the binding kinetics, but with a focus on residence time and its role in drug optimization. Molecular dynamics (MD) simulations and related methods are particularly relevant here because MD has emerged as one of the most suitable theoretical frameworks for developing computational approaches to kinetics (10–12). We will also discuss kinetic Monte Carlo (MC) as applied to biological and pharmacological systems. We conclude by arguing that the time has come for drug discovery to include a systematic optimization of the kinetics of binding and unbinding. This may help in predicting drug efficacy in vivo, thus reducing attrition rate in the long, costly process of bringing a new medicine to patients.
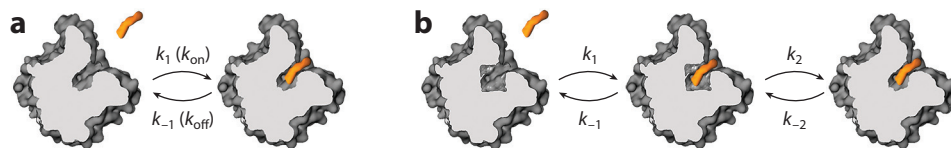

Figure 1

Schematic representation of protein-ligand binding mechanisms and associated kinetic constants. (*a*) The drug binding to its biological target is described by a single, one-step process characterized by the association and dissociation rate constants $k_1(k_{on})$ and k_{-1} (k_{off}). (*b*) A more general portrayal of the drug-binding process, where the target may undergo protein conformational changes and/or isomerization. In this case, a multistep mechanism is involved, and the on and off rates become a more complex function of the microscopic constants k_1, k_{-1}, k_2, and k_{-2}.

2. THEORETICAL BACKGROUND

The characterization of rate processes is of ubiquitous importance and has been handled by many theoretical works. An extremely good and extensive, although not recent, review of the different theoretical approaches can be found in the work of Hänggi et al. (13).

The theory of rate processes considers the frequency, and thus the corresponding probability, with which a system moves between two or more states, described by suitable combinations of the degrees of freedom of the system. Modeling these interconversions becomes relevant when they take place over a long timescale when compared to the dynamic timescales that characterize the states of local stability, that is, when the energetic separating barriers are of significant amplitude. For instance, in the case of atomistic systems described at the classical level, their direct simulation via advanced simulation techniques, such as MD, is limited in cases where the involved energetic barriers are so high as to make a statistically significant sampling of the transitions impractical or even infeasible.

2.1. Transition State Theory

Theoretical models of rate processes have historically focused on the prediction of kinetic rates based on the height of the separating energy barriers. Seminal works by van't Hoff (14) and Arrhenius (15) identified a linear correlation between the logarithm of reaction rates k and the inverse temperature $\beta = (k_B T)^{-1}$, where k_B is Boltzmann's constant and T the absolute temperature. The relationship therefore has the general form $k = \nu \exp(-\beta E_B)$, where E_b is the height of the barrier to overcome to escape a local stability energy basin and ν is a proportionality constant. Intuitively, it soon became clear that leaving the metastable state could be due to noise-assisted hopping events. However, a more quantitative description was made possible only by the development of theories describing fluctuations, such as Brownian motion. The idea of overcoming an energetic barrier was further clarified and formalized in the 1920s by Farkas (16), who characterized the rate of escape from a metastable state via the flux of particles that pass through the bottleneck separating products from reactants. At the same time, simple differential models involving the concentration of reactants (R) and products (P) as well as the kinetic rates were developed for the description of first- ($R \rightarrow P$, $\frac{dc_R}{dt} = -k\, c_R$) and second-order ($R_1 + R_2 \rightarrow P$, $\frac{dc_{R_1}}{dt} = -k_{bim}\, c_{R_1} c_{R_2}$) reactions (17–19). Here, the kinetic rates are the fundamental parameters describing the time evolution of the concentration of the species. In the 1930s, the nature of the proportionality constant ν was further clarified, leading to the Eyring-Polany expression for the rate constant (20):

$$k = \varkappa \frac{k_B T}{h} \frac{Z_{act}}{Z_a} \exp(-\beta E_b) \equiv \varkappa k_{TST}, \qquad \qquad 1.$$

where h is Planck's constant. Eyring derived this expression in the case of a nonlinear decomposing molecule comprising n atoms, with the rate expressed in terms of quantities that are available from the underlying potential surface. The partition function of the metastable reactants' state (Z_a) and that of the activated complex (Z_{act}) were derived by quantum statistical mechanics considerations. The concept of the activated complex is intrinsic to the kinetic theory and had already been hypothesized by Arrhenius (15). It is often used interchangeably with that of the transition state. However, the transition state represents only the highest energy configuration(s) of the system during the reaction. In contrast, the activated complex includes several configurations near the transition state that the system can undergo during the transformation from products to reactants. Importantly, although several key ingredients of the original proportionality constant are elucidated in Equation 1, a further constant, $\varkappa$, still remains. This is the transmission coefficient and it accounts for those reactive trajectories that recross the transition state and return
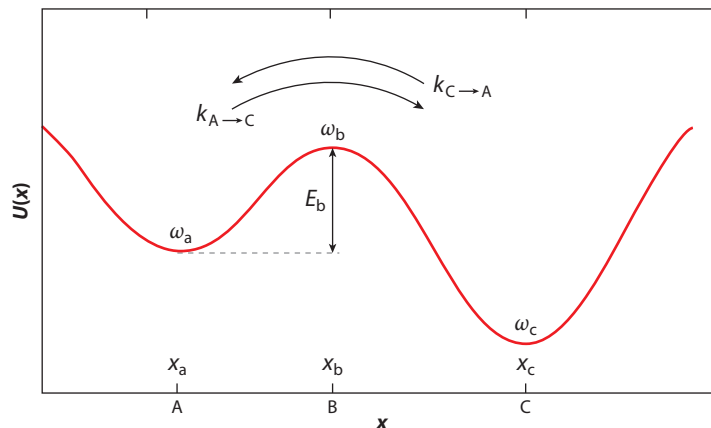
Figure 2

Double-well potential energy function along a generic reaction coordinate x. Two metastable states are found, A and C, characterized by the angular frequencies ω_a and ω_c, respectively. The rate for the A to C transition $k_{A \to C}$ is related to the height of the activation energy E_b separating the two energy wells through the transition state B.

without ending in the products state. Consequently, its value is always between 0 and 1. When $\varkappa$ is assumed to be 1, which is a common assumption, the transition state theory (TST) rate k_{TST} is recovered. Most of the successive work in this area focused on studying the complex behavior of the transmission coefficient in different kinds of systems and situations.

It is possible to provide some numerical answers to the question of this behavior by means of the reactive flux formalism, in which dynamical corrections are calculated from dynamical trajectories initiated at the transition state (21, 22).

2.2. Kramers Rate Theory

To better illustrate the framework within which the TST and more advanced theories were later derived, we shall here consider the underlying assumptions and mathematical formalisms in more detail.

Let us consider two macrostates A and C of local stability, as shown in **Figure 2**. For instance, A can collect the microstates where the reactants are not bound while C contains those corresponding to the formed product. Let us also assume that x is a one-dimensional collective variable, that is, a combination of degrees of freedom of the system, able to correctly represent the progress of the considered process, including whether the system belongs to the different states of interest. Then, the time evolution of the process is represented by that of the reaction coordinate $x(t)$.

If we consider a system in the so-called canonical ensemble, it is coupled to the thermal bath, which maintains constant the thermodynamic temperature T. The average interaction of the system with the countless degrees of freedom of the thermal bath can be, under some assumptions, modeled as the combination of a white background Gaussian noise and a viscous drag affecting the motion of all the particles making up the system itself. The evolution equations for such a system, comprising N classical particles of positions, momenta, and masses $\mathbf{r}_i$, $\mathbf{p}_i$, and m_i, respectively, subjected to a potential energy U are therefore Langevin-like:

$$\begin{cases} \dfrac{d\mathbf{r}_i}{dt} = \dfrac{\mathbf{p}_i}{m_i} \\ \dfrac{d\mathbf{p}_i}{dt} = -\nabla_{r_i} U - \gamma_i \mathbf{p}_i + \sqrt{D_i} m_i \mathbf{n}_i(t), \end{cases} \qquad 2.$$

where γ_i and D_i are the viscous friction coefficient and the diffusion constant, respectively, accounting for the number of collisions occurring in the unit time. $n_{i,\alpha}$ are white, that is, δ-correlated, Gaussian noise terms whose statistical properties are described by the expectation values below:

$$\langle n_{i,\alpha}(t) \geq 0, \; < n_{i,\alpha}(t_1) n_{j,\beta}(t_2) \rangle = 2 \, \delta_{i,j} \, \delta_{\alpha,\beta} \delta(t_1 - t_2). \qquad 3.$$

Due to the presence of the noise, Equation 2 is a stochastic differential system whose treatment needs suitable mathematical tools and whose solutions (i.e., the coordinates and momenta as a function of time) are stochastic processes.

The Fokker-Planck equation describes the evolution of the probability density W for positions and momenta that are the solution of the stochastic dynamical system of Equation 2 (23) and has the following form:

$$\frac{\partial W(\mathbf{r}, \mathbf{p})}{\partial t} = \sum_{i=1}^{N} \sum_{\alpha=1}^{3} \left\{ \frac{\partial U(\mathbf{r})}{\partial r_{i,\alpha}} \frac{\partial W}{\partial p_{i,\alpha}} - \frac{p_{i,\alpha}}{m_i} \frac{\partial W}{\partial r_{i,\alpha}} + \gamma_i W + \gamma_i p_{i,\alpha} \frac{\partial W}{\partial p_{i,\alpha}} + D_i m_i^2 \frac{\partial^2 W}{\partial p_{i,\alpha}^2} \right\}. \qquad 4.$$

The different contributions to the evolution of the system can easily be identified. The first two addends in the right-hand side of Equation 4 descend from the usual Hamiltonian dynamics, that is, those described by the Liouville equation. The third and fourth terms are due to the viscous drag. The final term is caused by the noisy force. If we use the following form of the Einstein-Smoluchowski relationship to connect the diffusion and the friction coefficients:

$$\gamma_i = \frac{D_i m_i}{k_B T}, \qquad 5.$$

we observe that Equation 4 admits the Boltzmann distribution as a stationary solution. According to these dynamics, the average total energy of the system is constant, as the energy injection is balanced by the noise and energy dissipation via the friction.

In this context, the collective variable $x(t)$ also becomes a random process, whose dynamics is made mathematically more tractable by a number of simplifications. These simplifications involve contracting the complete phase space dynamics of the system plus the thermal bath, averaging the effect of the interactions leading to thermal equilibrium, and then considering the dynamics of a single collective variable, ruled by a mean force potential, averaging over all the other degrees of freedom. Rigorously, projecting the entire dynamics in full phase space onto that of much reduced dimensions originates a non-Markovian dynamics in the reduced space (24, 25). A Markovian description, such as that provided above, can be recovered under the assumption that the correlation time of the noise is extremely short. Most of the mathematical derivations presented here rely on a separation of timescales: The correlation time of noise should be much shorter than the relaxation time of the system back into every single attraction basin, which should in turn be shorter than the time of escape from those basins.

In this context, the dynamics of escape is connected to the acquisition of the energy necessary to reach the top of the barrier, that is, the activated state region. Then, the system must lose energy to become trapped inside the neighboring well C. The timescale needed to acquire this energy depends on the size of the fluctuations $x(t) - <x(t)>$, which in turn depends on the strength of the noise, quantifiable via $k_B T$. In the end, the escape event can be considered frequent if $E_b \beta \ll 1$, with E_b being the height of the barrier to be overcome.

The Kramers derivation relies on the assumption that the dynamics of the collective variable also follows a Langevin evolution equation, similar to Equation 2:

$$\frac{d^2 x(t)}{dt^2} = -\frac{dU^{eff}(x)}{M dx} - \gamma \frac{dx(t)}{dt} + \sqrt{D} n(t); \quad -\frac{dU^{eff}(x)}{M dx} = \frac{F^{eff}(x)}{M}; \quad \gamma = \frac{DM}{k_B T},$$ 6.

where M is the effective mass associated with the collective variable; U^{eff} is the effective potential ruling the dynamics of the process; and F^{eff} is the corresponding force.

Based on the model and relationships shown in Equation 6, the strength of the interaction between the reaction coordinate and the remaining degrees of freedom is basically ruled by the damping rate γ. Under these assumptions, and by means of some involved mathematical derivations that go beyond the purposes of this review, Kramers (26) derived two main analytical expressions for the kinetics of the exchange between the A and C states crossing a barrier at the transition state B.

The first expression holds for moderate-to-strong values for the friction, when the system is said to be in the spatial-diffusion regime:

$$k_{A \to C} = \varkappa \frac{\omega_a}{2\pi} \exp(-\beta E_b) = \left[\sqrt{\left(\frac{\gamma}{2\omega_b}\right)^2 + 1} - \frac{\gamma}{2\omega_b} \right] \frac{\omega_a}{2\pi} \exp(-\beta E_b) \underset{\gamma \gg \omega_b}{\to} \frac{\omega_a \omega_b}{2\pi \gamma} \exp(-\beta E_b).$$

7.

Here, ω_a and ω_b are the angular frequencies corresponding to a local quadratic approximation of the energy around the minimum of the starting attracting basin, and around the transition state, respectively. The limit corresponds to the so-called overdamped regime:

$$U(x) \approx U(x_a) + \frac{1}{2}\omega_a^2 (x - x_a)^2;$$ 8.

$$U(x) \approx U(x_b) - \frac{1}{2}\omega_b^2 (x - x_b)^2 \equiv E_b + U(x_a) - \frac{1}{2}\omega_b^2 (x - x_b)^2.$$ 9.

Interestingly, for a given height of the energy barrier, the rate increases with the steepness of the barrier itself.

In the alternative case of low damping rate (corresponding to the so-called energy-diffusion regime), the Kramers treatment leads to the following expression for the escape rate from the basin A, having a barrier of height E_b:

$$k_{A \to C} = \gamma \beta I(E_b) \frac{\omega_a}{2\pi} \exp(-\beta E_b).$$ 10.

The derivation used by Kramers envisions the injection of particles into the starting basin A of the energy landscape. In the case of low friction, each particle does not relax immediately into A but rather may go back and forth before landing into one basin. In this case, the right-hand side of Equation 10 must be multiplied by the probability that the landing and thermalizing occur in basin A and from that point the process of escape takes place. Another relevant aspect of Equation 10 is the presence of the action variable, which is the following integral calculated on a closed path of the collective variables (CVs) at energy E_b, that is, at the top of the barrier:

$$I(E_b) \equiv \oint p dq.$$ 11.

The presence in the equation of the value of the action at the barrier energy implies that, for the energy-diffusion controlled situation, the anharmonic part of the well also affects the kinetic rate.

There have been several attempts to find an interpolating expression for intermediate values of friction. Interestingly, Tiwary & Berne (27) recently used an enhanced sampling technique named infrequent metadynamics to characterize this intermediate regime, albeit in a numerical fashion.

2.3. Path-Sampling Methods

The above approaches strive to obtain analytical estimates of kinetic rates based on underlying energy profiles and different environmental conditions. In contrast, path-sampling methods are an interesting, albeit time- and resource-demanding approach to obtaining numerical estimates of free-energy profiles and kinetic rates. The development of path-sampling methods was made possible by the availability of increased computational resources. Here, we will only scratch the surface of this interesting class of methods, without any claim of completeness.

Path-sampling methods rely on the idea that rare events per se are not slow, just very infrequent. Therefore, these methods concentrate the computational effort on the transitional events only. They do this by collecting representative pathways, which constitute the transition path ensemble (TPE), where the system moves from different stable macrostates.

If the TPE represents the underlying dynamics well, it can be used to characterize the system's dynamics at a macroscopic level by computing rate constants. It can also be used to understand transitions at a microscopic level. A few examples of transition path methods are transition path sampling (TPS), transition interface sampling, forward flux sampling, direct forward flux sampling, and the branched growth sampling. Here, we briefly describe TPS. For a more extended and detailed view, the reader is referred to other sources (28–30 and references therein).

2.3.1. Transition path sampling. To obtain the TPE, TPS starts from a trajectory $\{\mathbf{X}_i^0, \ i = 0, 1, \ldots, L\}$ of length L (often obtained from brute-force MD), which connects the starting state A and the final state C in phase space. Let us assume that we have the characteristic function $\chi(\mathbf{r}, \mathbf{p})$ for states A and C as a function of the coordinates of the system, so that $(\mathbf{r}, \mathbf{p}) \in A \leftrightarrow \chi(\mathbf{r}, \mathbf{p}) \leq \chi_A$ and $(\mathbf{r}, \mathbf{p}) \in C \leftrightarrow \chi(\mathbf{r}, \mathbf{p}) \geq \chi_C$. Different trajectories connecting A and C are then derived from $\{\mathbf{X}_i^0\}$ by choosing at random an intermediate frame, say j, and starting one forward and one backward trajectory of length $L-j$ and j, respectively, with slightly perturbed momenta. The final joint trajectory is accepted according to a Metropolis-like probability:

$$P_{\text{acc}}\left(\{\mathbf{X}_i^1\}\right) = \ \Theta\left[\chi_A - \chi\left(\mathbf{X}_1^1\right)\right] \Theta\left[\chi\left(\mathbf{X}_L^1\right) - \chi_C\right] \min\left[1, \frac{\rho\left(\mathbf{X}_j^1\right)}{\rho\left(\mathbf{X}_j^0\right)}\right], \qquad 12.$$

where $\rho(.)$ is the equilibrium probability distribution in the phase space and $\Theta(\cdot)$ is the Heaviside step function.

If the rare transitions between the stable states A and C are separated by a single dynamical bottleneck, the correlation function of state populations in time, C(t), can be defined as the conditional probability of finding the system in the final region C at time t provided it started in A at time $t = 0$; that is,

$$C(t') = \ \frac{\Theta\{\chi_A - \chi[\mathbf{X}(t=0)]\}\,\Theta\{\chi[\mathbf{X}(t=t')] - \chi_C\}}{\Theta[\chi_A - \chi(\mathbf{X})]}. \qquad 13.$$

Under certain conditions and for times ranging between the molecular timescale and the reaction time [see Dellago et al. (29) for more details], this correlation is proportional to the rate constant from A to C: $C(t) = \ k_{A \to C}\, t$.

One of the shortcomings of TPS is that it requires knowledge of the state phase density and an initial reactive trajectory, which may not be realistically achievable. To address this, TPS variants and more advanced approaches have been developed. These go beyond the scope of the present work.

3. EXPERIMENTAL APPROACHES TO THE KINETICS OF DRUG BINDING

Historically, the efficacy of a drug has been evaluated in terms of its affinity toward specific molecular targets. Most of the effort has been directed toward developing methods and devising practical strategies to measure thermodynamic parameters, such as the equilibrium dissociation constant, K_d, and the half-maximal inhibitory concentration, IC_{50}. As a result, according to the specific problem under consideration, one can now choose from a great number of dedicated and established experimental techniques. Recent developments in drug discovery have raised awareness that characterizing kinetic properties can also be crucial when seeking to identify suitable novel drug-like molecules. In this context, the optimization of the association and dissociation rates has been the subject of much recent attention from the drug discovery community. The currently available methods for measuring these parameters rely on monitoring over time a specific signal that responds to the binding event. The literature describes several experimental techniques for determining the binding kinetics. These can be broadly classified into three classes: (*a*) assays that exploit a label for detection, (*b*) label-free techniques, and (*c*) assays based on enzyme activity (**Figure 3**). Below, we provide a general overview of the methods in these three groups, and report on how they have been applied to retrieve kinetic information related to ligand-target systems.

3.1. Labeled Methods

Radio- and spectroscopic labeling are the main options included in this first class. The former involves radiometric ligand binding assays, while methods based on spectroscopic detection rely
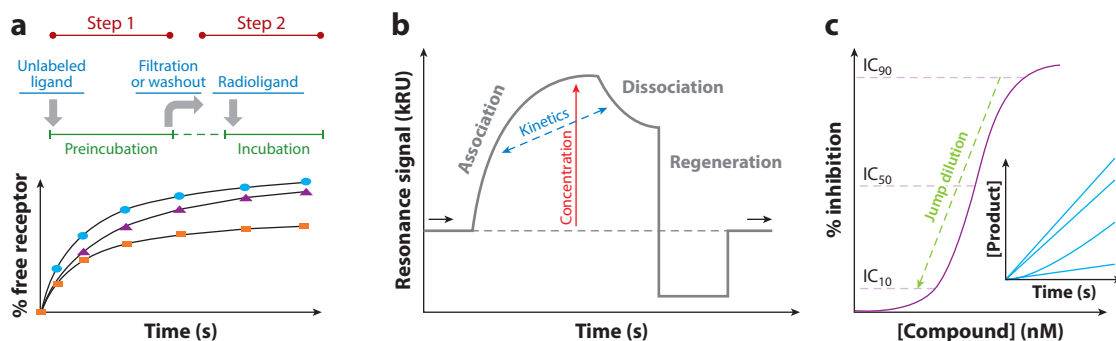

Figure 3

Major classes of experimental methods to measure binding kinetic rates. (*a*) Sample pipeline followed in indirect radiometric binding assays. The plot displays a typical target occupancy against time. (*b*) Time-dependent response curve as obtained in surface plasmon resonance workflows, with detail about complex formation/disruption on the sensor surface. (*c*) Schematic representation of a jump-dilution procedure displayed over the concentration-response curve of an enzymatic assay. Typical progress curves produced are reported in the inset. Abbreviations: IC_{50}, half-maximal inhibitory concentration; kRU, kilo response unit. Data from References 33, 57, and 75.

mostly on fluorescence. A radiolabel is essentially the presence of radioactive isotopes in the molecule that we wish to track. During their decay to a more stable state, these isotopes emit radiation, which can be detected to monitor the labeled species. In radiometric binding assays, ligands are typically tagged to follow the time course of their interaction with the molecular targets. Radioligands can be exploited to perform saturation, competition, and kinetic assays (31). This allows the determination of the affinity in terms of K_d, the equilibrium inhibitor constant K_i of an unlabeled ligand, and kinetic rates. The literature contains several implementations of radiometric assays. These can be broadly divided into direct and indirect strategies (32, 33). In the direct approach, the concentration of the radioligand bound to the receptor of interest is followed over time, allowing for the measurement of its association and dissociation rate constants k_{on} and k_{off} (31). In indirect approaches, the ligand of interest is unlabeled. Instead, the competitive binding of a radioligand is exploited to determine the kinetic rates. Two popular implementations of this strategy are the method devised by Motulsky & Mahan (34) and the delayed association method (35, 36) (**Figure 3a**). The former is based on coincubation of the unlabeled compound and the radioligand with the molecular target before detection. It allows for the estimation of k_{on} and k_{off}. Notably, this strategy was recently modified in the dual-point competition association assay to perform high-throughput kinetic screening studies (37). In the delayed association method, a saturating concentration of the unlabeled ligand is preincubated with the receptor. The k_{off} can then be determined by monitoring the target occupancy by the radioligand that is subsequently added.

The direct approach is the most straightforward. Nevertheless, it requires the labeling of each ligand under consideration, which is expensive and labor intensive. In addition, not all drugs make good radioligands. This is also a rather low-throughput approach. In contrast to indirect methods, the ligands of interest are unlabeled, and only one radiolabeled species is required to carry out the assay. This makes larger-scale applications feasible, so indirect strategies are typically preferred. One advantage of radiometric binding assays is that no purification of the molecular target is necessary; in other words, they can be applied to readily available samples. Therefore, although alternative strategies are being explored, this has long been the preferred method for studying ligand binding to G protein–coupled receptors (GPCRs) (33). Indeed, maintaining the receptor in its native membrane environment avoids the alteration, and even complete loss, of its structure and function, which is essential for a reliable assay.

Ligands are labeled with fluorescent tags in spectroscopy-based approaches. After absorbing electromagnetic radiation at a certain wavelength, fluorophore groups emit at characteristic, generally longer wavelength values. As the radiation source stops, the emission ceases almost immediately. This physical principle is exploited in various assays in which the emitted radiation is recorded to measure ligand-receptor binding quantities. Notably, by taking advantage of the existing approaches, both k_{on} and k_{off} can be measured. It is possible to identify two general setups (38) (**Figure 3a**). In the first setup, one monitors the change in a fluorescence property upon binding of the labeled ligand to the molecular target. Parameters such as intensity (39–42) or polarization (43–46) are usually considered options. The second setup is based on energy transfer. Here, a group from the protein, intrinsic but most frequently conjugated, acts as the donor and excites the probe on the ligand. This requires that the donor and the acceptor be in close proximity. The emission is generally observed only once the ligand has reached the bound state. In fluorescent resonance energy transfer (FRET), the donor is in turn another fluorescent group present on the receptor, which can transfer energy via a nonradiative mechanism to the acceptor label on the ligand (47, 48). The acceptor converts this energy into a fluorescent signal. The analysis can be distorted by short-lived background fluorescence due to buffer, proteins, chemical compounds, cell lysate, and so on.

This can be addressed with a time-resolved variant (TR-FRET), in which the detection is delayed to allow for the transient fluorescence to disappear (49–52). The radiation source can be a luminescent species that is able to emit as the result of a chemical reaction. A typical choice is the enzyme luciferase, which catalyzes the oxidation of the luciferin molecule with concomitant production of light. This principle is employed in bioluminescence resonance energy transfer (BRET), where the energy transfer takes place between the luminescent donor conjugated to the receptor and a fluorescent acceptor on the ligand (53–55). Notably, as no excitation source is involved, BRET is a valid alternative to fluorescent donors when dealing with cells that can be damaged by excitation light or that are photoresponsive. As with radiolabeling, it can be demanding to tag each compound of interest, so indirect procedures are typically pursued. One strength of fluorescence-based strategies is that the recorded signal is specific to the binding. Thus, since no separation between bound and unbound species is involved, no washing and filtration procedures are necessary, making the assay homogenous and more suitable for high-throughput applications.

3.2. Label-Free Techniques

With the rare exception of ligands with an intrinsic feature that provides the label, a probe must be joined to the molecule under consideration. As mentioned above, this can be expensive and labor intensive, so label-free assays can be valuable alternatives when applicable (32, 38).

The most widespread choice is surface plasmon resonance (SPR), which has long been used to characterize the binding kinetics of small molecules of pharmaceutical interest (56). The instrument essentially comprises a sensor surface that forms the floor of a flow cell, through which there is a continuous flow of an aqueous solution. The sensor is covered by a thin gold film, on which the receptor molecules are immobilized. When the mass lying over the sensor surface varies, a real-time change in the refractive index is observed. Thus, as the immobilized targets bind the ligand molecules, an increase in the refractive index is detected. A typical SPR workflow (**Figure 3b**) starts with the association phase, in which a sample containing the ligand is injected into the instrument. As the pulse of the compound continues, the detected signal increases, until a steady state is reached. This step is followed by a dissociation phase, during which sample injection stops and is replaced by a continuous flow of buffer. As a consequence, ligand dissociation from the surface-bound complex takes place, and a decrease in the signal is observed. Time-dependent response unit (RU) curves can be built from the recorded data, from which both affinity and kinetic properties can be obtained. Specifically, k_{on} and k_{off} can be derived from the association and dissociation portions of the curve, while multiple detections at increasing ligand concentrations can be recorded to measure the K_d from the RU observed at the steady states (56).

In a standard SPR setup, purified soluble proteins are typically required for the immobilization on the gold film. The applicability of this technique depends strongly on those two aspects, namely, purification and immobilization (9, 32, 38). With regard to immobilization, there are many methods to achieve the stable binding of the receptors on the gold film (57, 58). However, it is essential to bear in mind that the procedure might compromise the structure, conformation, or binding site accessibility (32). The purification aspect is more crucial for membrane-bound receptors. Indeed, SPR assays have been extensively applied to successfully characterize targets such as proteases (59, 60), phosphatases (61), and kinases (62). Conversely, when it comes to GPCRs and membrane proteins more generally, the receptor native functionality should be ensured by solutions such as solubilizing detergents (63–66) or reconstituted high-density lipoprotein particles (67–69). Finally, since ligands are typically analyzed in series, throughput is typically confined (9, 38).

In addition to SPR, other label-free alternatives, such as the surface acoustic wave method (70), have been considered to measure on and off rates. One appealing option is isothermal titration

calorimetry (ITC) (56). ITC has historically been a routine technique for characterizing thermodynamic properties related to ligand-receptor binding. In ITC, the heat produced by the binding reaction is detected by determining the thermal power necessary to maintain a zero-temperature difference between two cells, one containing the sample and one acting as a reference. Peaks of thermal energy are measured at increasing time intervals to produce a thermogram, which is then converted to a binding isotherm plot to measure relevant quantities such as K_d, the change in enthalpy, and the stoichiometry of the reaction (56). Interestingly, several declinations of ITC, such as kinITC (71) and MuITC (72), have been devised and explored in recent years to extend the analysis to include kinetics. The literature contains successful applications of these approaches to protein-ligand binding, where both association and dissociation rates were determined (71, 72). These efforts demonstrate the real potential of calorimetry-based methods to achieve a comprehensive characterization of both the thermodynamics and kinetics of the ligand-receptor binding process.

3.3. Assays Based on Enzyme Activity

While effective, the above approaches require either dedicated instruments (e.g., SPR hardware) or demanding setups (e.g., radiometric and fluorescence-based methods). Therefore, researchers are exploring more practical ways to gather useful kinetic quantities. Techniques based on enzyme activity (32, 73) represent one example. Here, the idea is to take established assays, which were designed to determine the activity of a specific enzyme, and use them to retrieve kinetic information. Typically, these assays are based on monitoring substrate consumption or product formation due to the enzymatic reaction (74), which usually involves parameters such as spectroscopic absorbance increase or decrease, respectively. One straightforward application to kinetics is Copeland's jump-dilution assay, which measures k_{off} values and thus the residence times of small molecule ligands (75). In this assay, the target is incubated with an excess of inhibitor, for which a regular dose-response relationship can be determined. Usually, a ligand concentration equal to tenfold the IC_{50} is used, which corresponds to achieving approximately 90% inhibition. After an elapsed time necessary to reach equilibrium, a proper quantity of activity assay buffer is added to achieve a 100-fold dilution (**Figure 3c**). Immediately after the dilution event, recording of the receptor activity as a function of time begins. Thus, a plot of the enzyme activity against time, known as a progress curve, is obtained (**Figure 3c**). The result is typically a linear function, whose slope provides information about whether the inhibitor's inactivation mechanism is reversible or irreversible. Moreover, the curvature of the initial portion of the curve depends on the compound's residence time (75). In the dilution conditions, no significant rebinding events are expected; thus the dissociation constant can be determined from the mathematical function describing the progress curve. The short assay development time is a strength of this approach. However, the analysis of the progress curve is effective, and particularly reliable, when used to characterize compounds with slow dissociation rates (73, 75, 76).

4. COMPUTATIONAL APPROACHES TO DRUG BINDING KINETICS

In drug discovery, the ultimate goal of molecular simulations is to reliably model the behavior of biomolecules displaying pharmaceutical relevance. The structural and dynamical features of these key species can then be extracted by determining the thermodynamic and kinetic properties to comprehensively characterize the system of interest. In recent decades, this effort has focused on thermodynamics, with the main goals being to estimate quantities such as equilibrium populations and energetics. Very recently, there has been growing interest in kinetics for drug discovery (1–3). While existing experimental methods are routinely used to measure kinetic quantities (see

Section 3) (32, 33, 38), these methods do not provide any mechanistic interpretation of the underlying process at the atomic level.

MD simulations can capture all the configurations of a system over time at atomic-level detail. In principle, they are therefore well suited to reconstructing the kinetics of biomolecular processes. Given a suitable potential energy function, molecular systems are evolved in time within an MD framework by integrating Newton's equations of motion for all of the atoms in the model (77). From the coordinates and velocities of each atom associated with a specific configuration of the system, it is possible to take a step forward in time, thus sampling the phase space in a deterministic fashion. This procedure involves the calculation of forces acting between pairs of atoms of the system. The time span over which we carry out the integration is called the timestep. Then, by repeating this procedure for a series of timesteps, we obtain many configurations of the system as a function of time. This is called an MD trajectory. Unfortunately, the processes that we are most interested in characterizing, that is, protein-ligand (un)binding, are slow and infrequent. These events take place on timescales that are difficult to access with conventional MD simulations (hereafter referred to as "plain MD") on current hardware architectures. They are therefore said to be rare. Thus, despite the advances in computer power that enabled the first successes with this method, other methods have been introduced. Below, we review how these methods and plain MD have been used to estimate the kinetics of protein-ligand (un)binding (**Figure 4**).

4.1. Direct Estimation of Rate Constant via Brute-Force Sampling

In principle, plain MD allows a straightforward determination of kinetic observables. A comment is required here on the so-called MD thermostats, and their use in MD simulations for kinetics studies. As a matter of fact, MD is often used to perform a simulation under the conditions of the canonical ensemble, where the interaction of a system with a thermal bath is accounted for by suitable algorithms that keep constant its temperature. These algorithms are called thermostats. While a basic requisite for a thermostat is to preserve the correct statistics of occupation of the visited microstates, which should tend to the Boltzmann distribution for simulations that are sufficiently long, the preservation of kinetics is not equally obvious. In brief, thermostat algorithms based on particle velocities randomization, especially when strong coupling is used, affect the kinetics of the simulation. In contrast, algorithms that operate by scaling the velocities yield transport properties that are statistically indistinguishable from those of the microcanonical ensemble, provided they envision a coupling to the kinetic energy of the entire system. We refer the interested reader, for instance, to the work of Basconi & Shirts (78) for extended discussion about this issue. With the due attention paid to these aspects, rate constants can be determined by simply counting the number of transitions from one stable state to another, divided by the effective time spent by the system in the first state (and vice versa; see **Figure 2**) (79). The mean residence time, which is the average time the system remains in the initial well, is then defined as the inverse of the rate constant. The mean first passage time is the time after which the system enters the second state, provided that it started from the former. Under the assumption of instantaneous transitions (leaving one state corresponds to entering the other without visiting any other metastable state), the mean residence time is equal to the mean first passage time (79).

Biologically relevant events occur at much longer timescales than typical MD timesteps, so the sampling is very computationally demanding. To reliably estimate the rate constants, many transitions from the two states must be collected. This requirement is not usually met in dynamic docking simulations, which aim to flexibly investigate protein-ligand binding, without achieving a rigorous determination of the thermodynamics and kinetics. Dynamic docking is thus suitable for
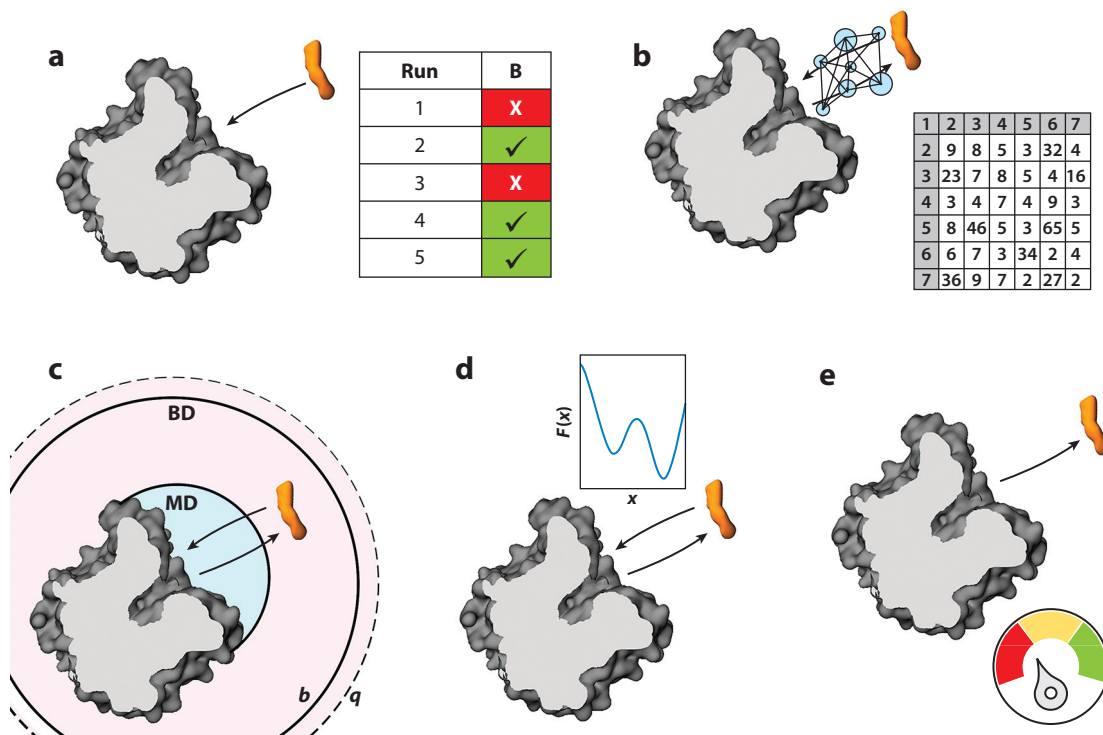
Figure 4

Schematic representation of the major computational approaches that allow the determination of protein-ligand binding kinetics. (*a*) Determination of k_{on} from the number of spontaneous binding events (B) over repeated runs of plain molecular dynamics (MD) simulations. (*b*) In Markov state models, kinetic rates are computed after constructing the transition probability matrix of the accessible microstates. (*c*) In multiscale approaches, the protein-ligand diffusive encounter modeled via Brownian dynamics (BD) is combined with an MD regime, which is applied once the partners are in close contact. (*d*) Free-energy surface (FES)-based biased approaches take advantage of a reconstructed FES to retrieve kinetics from biased simulations. (*e*) Kinetic information can also be obtained directly from biased simulations without necessarily passing for a converged FES.

industrial settings. Dynamic docking is based on MD. It investigates bimolecular recognition and binding, taking into account the full conformational flexibility of the molecular species. It thus overcomes the major limitations of conventional structure-based drug design methods, which are based on rigid molecular docking (80, 81). On the one hand, it is nowadays affordable to observe spontaneous binding events. This is because k_{on} values typically range from $10^3 \text{ M}^{-1} \text{ s}^{-1}$ to $10^9 \text{ M}^{-1} \text{ s}^{-1}$, with the latter corresponding to the rate limit of free diffusion. On the other hand, due to the long-lasting nature of protein-ligand interactions (k_{off} spans from about 1 s^{-1} to around 10^{-7} s^{-1}), it is currently infeasible to use plain MD to witness unbinding for drug-like molecules. However, instead of characterizing both rate constants, it is often sufficient to estimate either the on rate or off rate, depending on the specific problem one wishes to address. For example, rather than counting the transitions, it is a common choice to estimate the k_{on} from the frequency of binding over a series of repeated simulations (**Figure 4a**). Because of its reliance upon computational power alone, this strategy is usually referred to as brute-force sampling.

This approach has been followed since the earliest attempts at characterizing spontaneous protein-ligand binding via plain MD. The first examples were presented by the D.E. Shaw research group (82), which observed the association of dasatinib and PP1 to the Src kinase through

simulations in the low microsecond regime. A direct calculation of association rates was carried out by taking into account the frequency of binding and the concentration of ligands in the simulation box. Thus, k_{on} values of approximately 1.9 s⁻¹ mM⁻¹ and 4.3 s⁻¹ mM⁻¹ were estimated for dasatinib and PP1, respectively. Interestingly, in addition to reproducing the crystallographic pose, which was an impressive breakthrough at that time, the location of water molecules in the bound state was also correctly modeled. This procedure was extended to the β2 and β1 adrenergic receptors in the presence of known agonists and antagonists (83). For example, simulations of the β2 receptor with alprenolol, summing to approximately 60 μs, resulted in 12 full binding events. The direct calculation of the association rate constant was complicated by the tendency of the ligand to partition into the membrane. Taking this into account, a k_{on} of 3.1×10^7 s⁻¹ M⁻¹ was estimated, which is very close to the value of 1.0×10^7 s⁻¹ M⁻¹ reported in previous experiments.

Binding of the transition state analog DADMe-imucillin-H to purine nucleoside phosphorylase was also explored via brute-force MD (84). In 14 runs, which together aggregated to 13 μs of production, 11 binding events were recorded. All the trajectories were then parsed with a purposely developed machine learning algorithm. By integrating the available experimental data with details from the simulation setup, the expected mean first time to observe a binding event (i.e., a surrogate of the on rate) was estimated to be 246 ns. The same parameter was directly computed from the MD trajectories, resulting in a predicted value of 216 ns, which compared well with the expected value.

As previously mentioned, estimating the k_{off} for drug-like molecules through plain MD is not currently feasible. However, for small fragments, the weaker interactions established with the protein allow several unbinding events to be achieved within reasonable timescales. In this case, if enough statistics can be acquired, the dissociation rate constant can be obtained by fitting a single exponential (as required by a first-order kinetics) to the residence time correlation function, which can in turn be obtained by integrating the probability distribution $p(t_{unb})$ of the observed unbinding times (85):

$$C(t) = \int_t^\infty p(t_{unb}) \, d\tau. \qquad 14.$$

In this context, the spontaneous unbinding from the FK506 binding protein was explored for a series of fragment-like compounds, including dimethyl sulfoxide and chemicals of comparable size (86). Fifty independent MD simulations, lasting up to 20 ns, were initiated with the ligands in the bound state. Dissociation was expected within short simulation times, given the low affinity measured in the millimolar range. Several unbinding events were recorded, and a first-order kinetics was recognized for all the species. Mean residence times were computed for each ligand by applying a single exponential fit to the residence time correlation function, obtaining values consistent within ligands of a similar size.

4.2. Markov State Models and Adaptive Sampling Approaches

Instead of producing a few long trajectories that may capture only a few occurrences of the processes under investigation, plain MD can be exploited with a purely statistical approach (**Figure 4b**); that is, information from a greater number of shorter trajectories can be aggregated to construct a Markov state model (MSM) (87–90). The advantage is that several MD simulations can be run in parallel. Thus, while it is still crucial to adequately sample the entire configurational space (i.e., through brute-force sampling), it becomes much more manageable with this approach.

Briefly, to construct an MSM, one determines a transition probability matrix of the n sampled microstates. First, these microstates are defined based on geometric criteria through a clustering procedure on the sampled configurations. In the subsequent state decomposition phase, each configuration is assigned to the corresponding microstate. Thus, each trajectory is converted from a series of structures over time into a series of microstates over time, obtaining what are called the discrete trajectories. Discretization of the state space is a feature specific to MSM not shared by other methods that rely on fragmented trajectories (e.g., milestoning). Subsequently, jumps of fixed length are performed over each discrete trajectory and the transitions observed in the microstate space are stored in an $n \times n$ count matrix ($\mathbf{C}$). The size of the jumps, or lag time τ, is a multiple of the frequency at which trajectories are saved. The lag time defines the highest timescale resolution allowed to the model. Finally, $\mathbf{C}$ is converted into a transition probability matrix $\mathbf{P}$. Through diagonalization of $\mathbf{P}$, the scalar values λ_i for which the equation

$$\mathbf{P}\mathbf{v}_i = \lambda_i \mathbf{v}_i \qquad\qquad 15.$$

has nontrivial solutions $\mathbf{v}_i$ can be determined. These eigenvectors $\mathbf{v}_i$ describe specific transitions of the system (including binding and unbinding). The timescales t_i at which such motions occur can be recovered from the corresponding eigenvalues λ_i according to:

$$t_i = -\frac{\tau}{\ln \lambda_i}. \qquad\qquad 16.$$

The serine protease trypsin and reversible competitive inhibitor benzamidine provide a suitable test case for using MSMs to study binding processes. The protein is of modest size; the ligand displays low structural complexity; and experimental binding rates $k_{\mathrm{on}} = 0.29 \times 10^8$ M^{-1} s^{-1} and $k_{\mathrm{off}} = 0.06 \times 10^4$ s^{-1} (91) can be used to validate the predictions. In the first work reported by Buch et al. (92), 187 full binding events were observed in 500 plain MD runs, corresponding to nearly 50 μs of simulations. First, simpler models were constructed to recognize relevant metastable states and rate-limiting transitions. Then, a finer variant, built from the ligand Cartesian coordinates, was constructed to determine binding affinity and kinetic rates. Through a simple two-state model and assuming first-order kinetics, $k_{\mathrm{on}} = 1.5 \times 10^8$ M^{-1} s^{-1} and $k_{\mathrm{off}} = 9.5 \times 10^4$ s^{-1} were estimated.

The trajectories from Buch et al. (92) were subsequently integrated with additional plain MD (93), thus obtaining 543 runs, corresponding to approximately 150 μs. An MSM was first constructed based on distances between trypsin residues. It was further refined according to a cutoff distance of 6 Å between benzamidine and the binding site. This allowed protein conformational states to be distinguished from the advance of the binding process, resulting in a kinetic network comprising six unbound, four associated, and seven bound states. Binding rates were calculated from the mean first passage times, resulting in $k_{\mathrm{on}} = 6.4 \times 10^7$ M^{-1} s^{-1}, which compared well with experiments. In contrast, $k_{\mathrm{off}} = 131 \times 10^2$ s^{-1} was overestimated by approximately two orders of magnitude.

An interesting feature of MSMs is the possibility of identifying the microstates for which additional sampling is required, thus guiding an exhaustive exploration of the configurational space. This procedure, termed adaptive sampling (94–97), allows the quality of the model to be progressively improved. However, human supervision is typically required to carry out resampling. To overcome this requirement, Doerr & De Fabritiis (94) devised an automatic, iterative, and on-the-fly approach to efficiently determine where best to sample from. Testing on the trypsin-benzamidine system, the kinetic rates $k_{\mathrm{on}} = 4.4 \times 10^8$ M^{-1} s^{-1} and $k_{\mathrm{off}} = 2.8 \times 10^4$ s^{-1} were computed (94). Notably, with less than 1 μs gathered, this approach obtained the same accuracy as results from 8-μs-long aggregated trajectories and conventional MSMs.

Methodologies relying on adaptivity ensure the occurrence of infrequent events while optimizing the computational effort. Indeed, this capability of guiding the dynamics toward relevant regions of the phase space is a more general idea, not exclusive to MSM. Common to the different approaches is nevertheless the aggregation of large trajectory pools obtained via unbiased sampling to achieve a statistical interpretation of biological phenomena. Within this context, adaptive multilevel splitting (98) has recently found application in protein-ligand binding. Specifically, branching points from which additional simulations can be launched are adaptively identified from parent trajectories that start in the bound state. As a result, an ensemble of reactive paths leading to protein-ligand dissociation is obtained and the average reactive path time can be computed. By testing on the prototypical trypsin-benzamidine system, the mean first passage time could be estimated by considering the time spent in nonreactive trajectory loops and in reactive paths (99).

Another guided dynamics framework proposed by Dickson & Brooks (100) depends on the assignment of specific weights to an ensemble of unbiased trajectories. Such a weighted ensemble algorithm (WExplore) generates the pool of trajectories through a series of merging and cloning operations according to a hierarchical scheme (100). On the one hand, unlike MSM, the method is not settled on Markovian assumptions. On the other hand, it shares with MSM the possibility of interpreting the MD trajectories through a conformational space network, which can be further visualized and analyzed. Within this strategy, the unbinding rate is estimated from the sum of the weighted passage times associated with the collection of all reactive trajectories. The method has gradually found application at increasing levels of complexity, comprising the binding of low-affinity ligands (101), the trypsin-benzamidine system (102), and the dissociation process of a drug-like molecule from the soluble epoxide hydrolase protein (103). Notably, in the latter case, an experimental residence time of 11 minutes was accessed by aggregating only 6 μs of simulation. Moreover, the approach has also found extension in the enhanced sampling field (104).

4.3. Brownian Dynamics and Multiscale Modeling

When performing MD, each atom of the system is evolved in time according to Newton's second law of motion, producing atomic-scale resolution trajectories. More generally, however, the dynamics of a solute immersed in a solvent can be described by the Langevin equation of Equation 2 (105). In Langevin dynamics, the solvent is not explicitly included, but hydrodynamic effects on the solute are modeled through γ, which is the friction coefficient describing the medium viscosity, and $R(t)$, a random force that acts by agitating the body in a stochastic manner. In the limit of $\gamma = 0$, and with no random forces acting on the solute molecules, Newton's equations of motion are recovered. Conversely, in the limit of infinite γ, a diffusive regime is envisaged, whereby the motion of the solute particles is slow, and the inertial memory is rapidly lost. This leads to the approximate Langevin equation for overdamped regimes, or Brownian dynamics (BD) (106):

$$\frac{\partial x}{\partial t} = -\frac{\partial U(x)}{\gamma \, \partial x} + \frac{R(t)}{\gamma}. \qquad 17.$$

The BD formalism reduces per se the computational burden, as only the solute is described at the atomistic level, while the solvent is treated through appropriate implicit models of solvation (107). Moreover, in BD molecular simulations, the solute molecules are generally modeled as rigid bodies, where only translations and rotations are allowed. As a result, by neglecting internal degrees of freedom, larger timesteps are allowed and the simulation performance improves significantly.

An example of BD simulations is provided by Sung et al. (108) in their investigation of the binding of the natural substrate sialic acid and the inhibitor oseltamivir to the neuraminidase glycoprotein. By taking advantage of a massive number (to the order of 10^8) of BD runs, second-order

association rates were computed from the rotational and translational diffusion constants and from the fraction of simulations leading to productive complexes (109). In particular, following the pioneering work by Northrup et al. (109), two dividing surfaces are introduced in the simulation domain centered on the receptor: a *b*-surface separating the inner region of anisotropic interactions from the isotropic outer region, and a *q*-surface where trajectories are interrupted. Thus, the effective on rate can be factorized as:

$$k_{\text{on}} = k_{\text{D}}\,(b)\,p \qquad\qquad 18.$$

where $k_{\text{D}}(b)$ is the diffusion-limited rate constant at which the ligand encounters the *b*-surface irrespective of subsequent binding, while *p* accounts for the probability commitment of trajectories hitting the *b*-surface to bind rather than escape to infinite separation (*q*-surface), which is related to the intrinsic rate constant of binding (110). The former quantity can be estimated analytically by relying on continuum theories (111) or by considering forces and hydrodynamic interactions. The latter quantity must be extracted from BD trajectories. Following this approach, the computed $k_{\text{on}} = 5.17 \times 10^6$ M^{-1} s^{-1} for oseltamivir compared well with the reference experimental $k_{\text{on}} = 2.52 \times 10^6$ M^{-1} s^{-1}.

BD allows more statistics associated with slow processes to be collected. However, there is generally also a loss of resolution of smaller-scale events, such as local rearrangements of the solutes. One interesting variation of BD is its inclusion in a multiscale framework to recover relevant kinetic quantities, while maintaining an atomistic resolution in relevant regions of the simulation domain. Multiscale modeling is a more general concept in science, whereby problems are solved by integrating information obtained at multiple scales (112, 113). Similarly, recently developed multiscale methods combine the use of MD and BD (114, 115) (**Figure 4c**). In the context of binding processes, the general idea is to use less demanding BD to treat the diffusive encounter of the involved species, while switching to MD to model their behavior once they are in close proximity.

Zeller et al. (116) combined MD and BD in a multiscale approach to study the association with binding of the inhibitors oseltamivir and zanamivir to H1N1 neuraminidase. The MD regime was limited to a cone protruding up to 32 Å outside of the binding site entrance. A spherical surface at 12 Å, from which the MD runs were launched, was defined as the protein-ligand encounter surface (ES). Additionally, BD simulations (*b*-surface) began from a spherical shell set at 60 Å around the protein. The *q*-surface was set at 100 Å. Roughly 1,200 MD runs, for approximately 85 μs (50.0 μs for oseltamivir and 35.7 μs for zanamivir), were started from the ES, while two sets of 10^6 BD trajectories were executed. By considering the Smoluchowski diffusion-limited rate constant and integrating the BD and MD regimes in the estimation of *p*, k_{on} values were computed in reasonable agreement with experiments for both inhibitors. Interestingly, MD-based information enters Equation 18 as the probability that trajectories started at the ES will not escape the MD region within 2 μs of sampling. From this standpoint, the atomistic portion of simulative endeavor is reminiscent of a brute-force sampling strategy.

Conversely, the Simulation Enabled Estimation of Kinetic Rates (SEEKR) package developed by the Amaro group (117) combines MD, BD, and milestoning theory in an integrated multiscale approach. In milestoning, the dynamics involved in a complex process are broken down into transition events between predetermined intermediates along a reaction coordinate (118, 119). These transition events are called milestones. Multiple simulations are run at each milestone to gather proper statistics and obtain stationary flux distributions (*q*) across each milestone, while making optimal use of computational resources (120). Indeed, besides the speedup intrinsically provided by multiscaling, the striking advantage in efficiency of this method is the possibility of running

the different milestones in parallel. Then, SEEKR assesses the diffusion-limited rate constant by considering forces and hydrodynamic interactions, while p is obtained by combining MD and BD fluxes through

$$p = \sum_z q_z, \qquad\qquad 19.$$

where z is the index of a milestone representing a bound state. Through this multiscale implementation, the association pathway of the trypsin-benzamidine system was broken down into 10 milestones placed at increasing radial distances, 1–14 Å, from the binding pocket. BD was used from the outermost milestone to farther regions as set, comprising 10^6 simulations, while the MD regime was applied to the innermost milestones, summing to approximately 19 μs. By combining the obtained data, $k_{on} = 2.1 \times 10^7$ M^{-1} s^{-1} and $k_{off} = 83$ s^{-1} were computed; these were in very good agreement with the experimentally measured $k_{on} = 2.9 \times 10^7$ M^{-1} s^{-1} and $k_{off} = 600$ s^{-1}.

The strategies discussed above rely on MD and BD to implement multiscale frameworks for the study of molecular kinetics. While such construction was a natural choice in view of a gain in efficiency, alternative combinations of methods can also be envisaged. For instance, a multiscale scheme including a nonclassical description was recently introduced (121). In this scheme, while biased MD simulations based on transition path sampling formalisms are employed to model the protein-ligand dissociation (see below) (122), the energetic and kinetic characterization can be subsequently refined through a QM/MM-based method (123). Notably, including the quantum level allows taking into account polarization effects, which are typically neglected in common force fields (124). In the application to study the binding process of imatinib to the Src kinase, a free-energy correction on relevant stations along the association pathway could be estimated, allowing in turn the determination of a dissociation rate in better agreement with experiments (121).

4.4. Free-Energy Surface–Based Biased Approaches

Despite the unquestionable power of MD in predicting kinetic parameters and providing atomic-level insights into molecular mechanisms, the sampling of slow processes is still a key challenge. Another class of MD-based methods has therefore been introduced to improve the exploration of the configurational space at a fully atomistic level, while keeping the computational effort as contained as possible (125). These methods are often referred to as biased MD, meaning that the observation of rare events is encouraged by introducing external forces [e.g., umbrella sampling (US) or metadynamics (MetaD)] that act on selected reaction coordinates (or CVs) or by using altered statistical ensembles [e.g., parallel tempering or scaled MD (sMD)] (77). These methods were devised to characterize thermodynamic features, essentially by reconstructing free-energy profiles (**Figure 4d**). Nevertheless, they are increasingly being used to retrieve kinetic information. This can be achieved by using a reconstructed free-energy surface (FES) or by directly taking advantage of the accelerated sampling of the slow event. In the latter case, specific frameworks are devised to extract kinetic quantities directly from the biased rates. These will be covered in the next paragraph. Conversely, once a free-energy profile has been obtained, one can attempt to directly calculate the kinetic rates by resorting to the arguments of TST or evolutions thereof. One such application, based on US (126, 127), focused on the dynamics of tetramethylammonium through the gorge of acetylcholinesterase, which gives access to the active site. Seven US windows spaced at 0.6 Å were placed along the distance between the protein center of mass and the ligand nitrogen atom in order to describe the advancement along the gorge and the final occupation of the binding site. Through 1 ns of sampling per window, a surprisingly low energy barrier of approximately 8–10 kJ mol^{-1} was found. Assuming a high friction regime and applying the Kramers modified TST

(105), the corresponding rate was directly calculated from the determined energy difference and the squared frequency of crossing the barrier, which was in turn calculated by the second derivative of the FES in the initial well. Conversely, the Kramer's transmission coefficient was scaled down to 0.17 in agreement with overdamped protein reactions (128). This allowed an incoming rate of 10^8 s^{-1} to be determined for the ligand, which is consistent with the fast reaction rate determined experimentally for acetylcholinesterase.

To the best of our knowledge, the previous example is the only report to date where kinetics information was recovered from a FES using a TST-like procedure. This strategy is widely used in several other contexts, such as the calculation of ion-water exchange rates (129, 130). However, it is generally understood that the complexity of protein-ligand processes mostly prevents such a direct approach. This is especially true when more than two basins are found in the FES. In these cases, it can be more convenient to exploit the FES to retrieve kinetic information by constructing a kinetic model, which is essentially an interpretation of the system dynamics in terms of its kinetic properties. In particular, the FES can be broken down according to a discrete-state scheme by subdividing the continuous reaction coordinate space into a grid of discrete bins (131). To this end, each reaction coordinate is partitioned into a series of blocks of fixed size, which define the side of the bin along that direction. Each bin is then assigned the corresponding free-energy value according to the previously reconstructed FES. Finally, assuming a Markovian diffusive behavior in the bin space, a matrix of transition rates is built. Specifically, the rates for transitions between each bin and its first and second nearest neighbors are computed from the free-energy difference between the bins and the diffusion matrix in the reaction coordinate space. The latter is obtained through a maximum likelihood procedure based on shorter, not necessarily converged, plain MD simulations. Once the model is constructed, a kinetic Monte Carlo (kMC) algorithm (132, 133) can be used to carry out dynamics in the bin space and from there to determine kinetic rates between states of interest at a different resolution level. Notably, the framework allows the identification of major kinetic attractors and the corresponding interconversion rates, thus providing a more comprehensive interpretation of the entire system dynamics. The whole procedure bears some resemblance to the discrete-state kinetics obtained through MSM in the context of plain MD, although here the rates are extracted by the features of the FES and the diffusion matrix.

The approach was applied to the binding process of a short peptide substrate associating with wild-type HIV-1 protease (134). 1.6 μs of bias-exchange metadynamics were executed (135), with 7 CVs providing a geometrical description of the process. Only 4 CVs were chosen for the binning procedure, as the remaining correlated to these. The diffusion matrix was determined from a 10-ns-long unbiased MD simulation. The model allowed the design of a kinetic network of the major intermediates, with $k_{on} = 1.26 \times 10^6$ M^{-1} s^{-1} and $k_{off} = 57.1$ s^{-1} computed. This is in line with experimental values for a close analog of the ligand.

In principle, FES-based biased methods can comprehensively describe the process under investigation, both qualitatively (by characterizing the relevant transition states) and quantitatively (provided that suitable approaches, such as TST, are available to derive kinetic rates from the FES). We note that kMC per se is not able to derive kinetic rates. Rather, it uses them as input to provide the global dynamics of the system, possibly at a coarser level of resolution. Specifically, kMC propagates the system from state to state according to the given rates by generating random first-escape times that obey the following exponential distribution:

$$p_{ij}(t) = k_{ij}\exp\left(-k_{ij}t\right), \qquad\qquad 20.$$

where i is the starting state and j spans each of the possible arrival states, that is, all the escape paths.

Methods based on reconstructing the FES have two major drawbacks. First, achieving a converged FES is not trivial, especially if several CVs are required to characterize the rare event. FES-based biased methods are therefore computationally intensive, although not as demanding as plain MD approaches. Second, and strictly related to the previous point, it is often difficult to devise the relevant CVs a priori. This can potentially introduce severe errors into the FES, which mostly affect the estimation of barriers. Moreover, the reduced representation of the phenomena in terms of collective variables will seriously affect the transmission coefficient, reducing the applicability of bare TST. Noteworthy, concerning this point, we mention an accurate but computationally expensive strategy to alleviate this behavior based on path CVs (136) and partial path transition interface sampling (PPTIS) (137). In the resulting procedure, called transition state-PPTIS (TS-PPTIS) (122), the free-energy profile is first characterized via metadynamics, while the diffusive barriers are subsequently refined by performing a series of unbiased MD simulations started around the transition states identified in the previous step (121, 138). In light of these considerations, alternative methods that can recover kinetic observables without the demanding and potentially error-prone FES are gaining increasing interest.

4.5. Biased Rates Approaches and Time-Rescaling Strategies

The introduction of external biases can be directly exploited to boost the dynamics of molecular systems. Transitions along slower degrees of freedom are facilitated, and rare events can be observed with increased probability, but the simulation time inevitably loses its physical meaning. This improved capability in exploring the configurational space can effectively be exploited to retrieve relevant kinetic information, as long as there is an appropriate strategy to rescale the biased rates (**Figure 4e**).

This idea has been successfully used to extend MetaD beyond the usual thermodynamic characterization (139). The devised procedure is based on two key elements. First, no bias must be released in the transition state regions. This requirement is met as long as the transition over this region is faster than the Gaussian deposition stride. As such, the procedure is mostly suited for systems characterized by rare but fast transitions. Because of the lowered frequency of bias introduction, the name infrequent metadynamics was coined. Secondly, basin-to-basin progressions need to be effectively monitored to assess that passage over a transition state has taken place. This is achieved by following the simulation time evolution of an acceleration factor, which undergoes noticeable kinks in response to transitions between minima. Notably, although there is no need to know the locations of energy minima in advance, it is nevertheless essential that the chosen CVs are able to effectively distinguish between stable basins. Within this framework, because no bias is added to the transition regions, the system can evolve according to a state-to-state sequence that preserves the unbiased dynamics. Therefore, by rescaling the MetaD simulation time with the acceleration factor, the true time can be recovered. Taking advantage of this procedure, the unbinding time is thus calculated as the average of the observed unbinding times after rescaling. Finally, taking the reciprocal of this unbinding time, the dissociation rate is obtained.

The procedure has been tested on the archetypal trypsin-benzamidine system (140). By reproducing 21 unbinding events using path CVs to guide sampling, a total simulation time of 5 μs was gathered, corresponding to approximately 3 s of real-time evolution. The direct computation of $k_{off} = 9.1$ s^{-1} was in fair agreement with the experimental value. Using the computed k_{off} together with the free-energy difference of binding from previous works, an indirect calculation of $k_{on} = 1.18 \times 10^7$ M^{-1} s^{-1} was pursued. Notably, the authors showed that 12 independent runs would suffice to obtain estimates of an equal level of accuracy. The protocol was subsequently applied to an inhibitor scaffold unbinding from its target p38 MAP kinase (141). Two sets of two CVs were

used, specifically the ligand-pocket distance and ligand solvation in the first case, and the path CVs as the second set. From 17 and 10 independent runs for the two sets, respectively, which together summed up to approximately 7 μs, $k_{off} = 0.02$ s^{-1} and $k_{off} = 0.04$ s^{-1} were determined, in good agreement with the experimental $k_{off} = 0.14$ s^{-1}. Notably, the consensus between the computed values highlighted how path CVs provided good estimations, despite not explicitly taking into account the ligand solvation.

In the optimization phase of a typical drug discovery pipeline, one is typically interested in identifying compounds with improved properties. Given the increasingly recognized relevance of kinetics, a common scenario involves identifying compounds with longer residence times. Here, simpler methods are desired, with fewer tunable parameters. To this end, a prioritization strategy is often sufficient to guide the optimization procedure. Accurate predictions of absolute values are not strictly necessary. In this context, a strategy based on MetaD has been proposed (142). The procedure allows a set of analog compounds to be discriminated according to their residence times toward a biomolecular target. A series of independent MetaD simulations is performed for each compound, starting from the bound complex and extending until the ligand achieves the fully solvated state. The average simulation time taken by each species is then computed.

Notably, in contrast to the common practice of using geometric criteria, the unbound state is defined in an energy-based manner. When the ligand is free to move in the solvent, no accumulation of deposited energy is expected to take place and the average value of the biased potential accumulated does not change much. Thus, this condition is set to assess that dissociation has occurred. To allow for this scheme to hold, the original implementation of MetaD is used, in which Gaussians of constant height are deposited at fixed time intervals. This allows for a proportional relation between the total bias deposited and the simulation time necessary to achieve full unbinding. The methodology was tested on a set of 10 arylpyrazole analogs inhibiting the CDK8 protein. For each compound, 14 independent runs were carried out, in which the dissociation event took place within a few tens of nanoseconds. The seven CVs were geometrical parameters that described rototranslational and conformational degrees of freedom of the ligand. Notably, these CVs are general enough to be adapted easily to other complexes. As a result, the compounds were successfully discriminated in three classes according to short, medium, and long residence times as observed in the experiments.

A different protocol to prioritize ligands according to their residence times is based on sMD but is similarly implemented (143). This biased method relies on the scaling of the entire potential energy surface, resulting in a smoothed profile in which energy barriers are lowered and transitions between energy minima are facilitated (144–146). However, at the scaling factor typically used (on the order of 0.4–0.5), protein structural stability can be compromised. Therefore, to prevent unfolding, gentle positional restraints are used on all backbone-heavy atoms, except for the residues in the binding pocket (143). A notable advantage of sMD is that one does not have to set a reaction coordinate to guide unbinding, because the potential scaling acts indistinctly on the entire system. The correlation with experimental dissociation rates can then be assessed by fitting to a simple linear function, after rescaling the computed unbinding times for the λ factor used. In the first published application, the pharmaceutically relevant targets HSP90 protein, GRP78 protein, and adenosine A2A receptor were considered (143). For each one, a different set comprising four known inhibitors was considered. By applying a scaling factor of 0.4, a total of 108, 84, and 80 runs were performed for HSP90, GRP78, and A2A, respectively, ranging from a few nanoseconds in the case of the fastest ligands to nearly 100 ns for the slowest. For all three targets, the inhibitors were ranked correctly in agreement with available experimental off rates. A subsequent study focused on a set of chemically unrelated activators of the glucokinase protein (147). In addition to being a further successful validation against a more heterogeneous class of ligands, the practical

effect of using a less aggressive scaling factor was investigated. This methodology is one of the modules of a commercial software named BiKi (short for binding kinetics) (148). It is currently used by pharmaceutical companies to prioritize compounds for chemical synthesis campaigns on the basis of residence time predictions.

We conclude this section by mentioning a further strategy to rank drug candidates by their computed residence time. This approach is based on random accelerated MD (RAMD), a form of biased dynamics without the definition of CVs. RAMD used mild random forces to promote the egress of ligands from their binding sites (149). When used to calculate relative residence times, this approach is known as τ-RAMD. With this strategy, Kokh et al. (150) recently correctly ranked the residence time of a large (70 compounds) set of diverse drug-like molecules bound to the HSP90 protein. This strategy obtained a good correlation ($R^2 = 0.86$) between computed and experimental residence times. It also highlighted salient features of the unbinding process that affected dissociation rates.

5. CONCLUSIONS

Lack of efficacy is one of the major factors behind the attrition rate in drug discovery. Despite remarkable in vitro affinity for a biological target, a drug is often unable to exert pharmacological and therapeutic effects in vivo. Besides the well-known issues related to absorption-distribution-metabolism-excretion (ADME), if a drug does not bind its biological target long enough, its efficacy in vivo may be compromised, and the probability of side effects increases. Therefore, the kinetics of drug-target binding and unbinding has emerged as a new in vitro parameter that may help predict drug efficacy in vivo. Several drug discovery programs have introduced residence time (the inverse of k_{off}) optimization as a new step in their pipelines. The optimization of residence times can have a positive impact on the highly costly developmental steps.

In the past few years, measurements of kinetic parameters have been increasingly implemented in the early stages of drug discovery. Here, we defined the three major categories of experimental techniques for these measurements and discussed their pros and cons in terms of drug discovery. We also presented in silico computational methods, which are increasingly used to assist the entire drug discovery process. We noted that there are currently no well-established computational methods for routinely predicting the kinetics of drug (un)binding. On the one side, there are fast methodologies for ranking compounds, although the accurate determination of absolute residence time values may require large training sets and robust correlations based on available experimental data. Still, these methodologies can be helpful in discerning fast from slow binders and in prioritizing compounds for chemical synthesis campaigns. On the other side, there are more accurate approaches for predicting the kinetics of drug binding. However, these approaches may require weeks or months of calculations and human labor to determine absolute residence time values for one single compound. Despite their high level of accuracy, these approaches are incompatible with drug discovery programs, which require a reasonable tradeoff between speed and accuracy.

In light of these considerations, we propose a combination of different sampling methods to estimate residence time. Fast approaches can be used for the initial ranking. They can be run in a few days or weeks to prioritize compounds for the subsequent stages of drug discovery. Additionally, these methodologies can point to relevant reaction coordinates (or path-related collective variables), which may then be used in more accurate approaches to identify minimum free-energy paths and calculate potentials of mean force. Thus, for a given objective, researchers can use the available arsenal of enhanced sampling methods to find the right compromise between speed and accuracy in the estimation, prediction, and eventually, accurate absolute calculation of the kinetics of drug binding/unbinding. This latter objective may still be affected by the

potentials used. However, there has been remarkable progress in recent years so that the goal of absolute thermodynamic and kinetic calculations for drug discovery now appears to be within reach.

DISCLOSURE STATEMENT

The authors are not aware of any affiliations, memberships, funding, or financial holdings that might be perceived as affecting the objectivity of this review.

ACKNOWLEDGMENTS

LITERATURE CITED

1. Pan AC, Borhani DW, Dror RO, Shaw DE. 2013. Molecular determinants of drug-receptor binding kinetics. *Drug Discov. Today* 18(13–14):667–73
2. Copeland RA, Pompliano DL, Meek TD. 2006. Drug-target residence time and its implications for lead optimization. *Nat. Rev. Drug Discov.* 5(9):730–39
3. Swinney DC. 2009. The role of binding kinetics in therapeutically useful drug action. *Curr. Opin. Drug Discov. Dev.* 12(1):31–39
4. Yin N, Pei J, Lai L. 2013. A comprehensive analysis of the influence of drug binding kinetics on drug action at molecular and systems levels. *Mol. Biosyst.* 9(6):1381–89
5. Tummino PJ, Copeland RA. 2008. Residence time of receptor-ligand complexes and its effect on biological function. *Biochemistry* 47(20):5481–92
6. Lu H, Tonge PJ. 2010. Drug-target residence time: critical information for lead optimization. *Curr. Opin. Chem. Biol.* 14(4):467–74
7. Zhang R, Monsma F. 2009. The importance of drug-target residence time. *Curr. Opin. Drug Discov. Dev.* 12(4):488–96
8. Copeland RA. 2016. The drug-target residence time model: a 10-year retrospective. *Nat. Rev. Drug Discov.* 15(2):87–95
9. Schuetz DA, de Witte WEA, Wong YC, Knasmueller B, Richter L, et al. 2017. Kinetics for drug discovery: an industry-driven effort to target drug residence time. *Drug Discov. Today* 22(6):896–911
10. Deganutti G, Moro S. 2017. Estimation of kinetic and thermodynamic ligand-binding parameters using computational strategies. *Futur. Med. Chem.* 9(5):507–23
11. Bruce NJ, Ganotra GK, Kokh DB, Sadiq SK, Wade RC. 2018. New approaches for computing ligand–receptor binding kinetics. *Curr. Opin. Struct. Biol.* 49:1–10
12. Bernetti M, Cavalli A, Mollica L. 2017. Protein–ligand (un) binding kinetics as a new paradigm for drug discovery at the crossroad between experiments and modelling. *MedChemComm* 8(3):534–50
13. Hänggi P, Talkner P, Borkovec M. 1990. Reaction-rate theory: fifty years after Kramers. *Rev. Mod. Phys.* 62(2):251
14. van't Hoff JH. 1884. *Etudes de Dynamique Chimique*. Amsterdam: Müller
15. Arrhenius S. 1889. On the reaction rate of the inversion of non-refined sugar upon souring. *Z. Phys. Chem.* 4(226):135501
16. Farkas L. 1927. Keimbildungsgeschwindigkeit in übersättigten Dämpfen. *Z. Phys. Chemie* 125(1):236–42
17. Lindemann FA, Arrhenius S, Langmuir I, Dhar NR, Perrin J, Lewis WCM. 1922. Discussion on "the radiation theory of chemical action." *Trans. Faraday Soc.* 17:598–606
18. Hinshelwood CN. 1926. *Kinetics of Chemical Change in Gaseous Systems*. London: Oxford Univ. Press/ Milford
19. Hinshelwood CN. 1926. On the theory of unimolecular reactions. *Proc. R. Soc. A* 113(763):230–33

20. Eyring H. 1935. The activated complex in chemical reactions. *J. Chem. Phys.* 3(2):107–15
21. Anderson JB. 1973. Statistical theories of chemical reactions. Distributions in the transition region. *J. Chem. Phys.* 58(10):4684–92
22. Chandler D. 1978. Statistical mechanics of isomerization dynamics in liquids and the transition state approximation. *J. Chem. Phys.* 68(6):2959–70
23. Risken H, Eberly JH. 1985. The Fokker-Planck equation, methods of solution and applications. *J. Opt. Soc. Am. B* 2:508
24. Kawasaki K. 1973. Simple derivations of generalized linear and nonlinear Langevin equations. *J. Phys. A Math. Nucl. Gen.* 6(9):1289
25. Grabert H, Hänggi P, Talkner P. 1980. Microdynamics and nonlinear stochastic processes of gross variables. *J. Stat. Phys.* 22(5):537–52
26. Kramers HA. 1940. Brownian motion in a field of force and the diffusion model of chemical reactions. *Physica* 7(4):284–304
27. Tiwary P, Berne BJ. 2016. Kramers turnover: from energy diffusion to spatial diffusion using metadynamics. *J. Chem. Phys.* 144(13):134103
28. Weinan E, Vanden-Eijnden E. 2006. Towards a theory of transition paths. *J. Stat. Phys.* 123(3):503
29. Dellago C, Bolhuis PG, Geissler PL. 2006. Transition path sampling methods. In *Computer Simulations in Condensed Matter Systems: From Materials to Chemical Biology*, Vol. 1. Springer, ed. M Ferrario, G Ciccotti, K Binder, pp. 349–91. Berlin: Springer
30. Escobedo FA, Borrero EE, Araque JC. 2009. Transition path sampling and forward flux sampling. Applications to biological systems. *J. Phys. Condens. Matter* 21(33):333101
31. Hulme EC, Trevethick MA. 2010. Ligand binding assays at equilibrium: validation and interpretation. *Br. J. Pharmacol.* 161(6):1219–37
32. Cusack KP, Wang Y, Hoemann MZ, Marjanovic J, Heym RG, Vasudevan A. 2015. Design strategies to address kinetics of drug binding and residence time. *Bioorg. Med. Chem. Lett.* 25(10):2019–27
33. Guo D, Hillger JM, Ijzerman AP, Heitman LH. 2014. Drug-target residence time—A case for G protein-coupled receptors. *Med. Res. Rev.* 34(4):856–92
34. Motulsky HJ, Mahan LC. 1984. The kinetics of competitive radioligand binding predicted by the law of mass action. *Mol. Pharmacol.* 25:1–9
35. Frost JJ, Wagner HN. 1984. Kinetics of binding to opiate receptors in vivo predicted from in vitro parameters. *Brain Res.* 305(1):1–11
36. Malany S, Hernandez LM, Smith WF, Crowe PD, Hoare SRJ. 2009. Analytical method for simultaneously measuring ex vivo drug receptor occupancy and dissociation rate: application to (R)-dimethindene occupancy of central histamine H1 receptors. *J. Recept. Signal Transduct. Res.* 29(2):84–93
37. Guo D, van Dorp EJH, Mulder-Krieger T, van Veldhoven JPD, Brussee J, et al. 2013. Dual-point competition association assay: a fast and high-throughput kinetic screening method for assessing ligand-receptor binding kinetics. *J. Biomol. Screen.* 18(3):309–20
38. Meyer-Almes FJ. 2015. Kinetic binding assays for the analysis of protein-ligand interactions. *Drug Discov. Today Technol.* 17:1–8
39. May LT, Self TJ, Briddon SJ, Hill SJ. 2010. The effect of allosteric modulators on the kinetics of agonist-G protein-coupled receptor interactions in single living cells. *Mol. Pharmacol.* 78(3):511–23
40. May LT, Bridge LJ, Stoddart LA, Briddon SJ, Hill SJ. 2011. Allosteric interactions across native adenosine-A3 receptor homodimers: quantification using single-cell ligand-binding kinetics. *FASEB J.* 25(10):3465–76
41. Gherbi K, May LT, Baker JG, Briddon SJ, Hill SJ. 2015. Negative cooperativity across B1-adrenoceptor homodimers provides insights into the nature of the secondary low-affinity CGP 12177 B1-adrenoceptor binding conformation. *FASEB J.* 29(7):2859–71
42. Bruno A, Lembo F, Novellino E, Stornaiuolo M, Marinelli L. 2015. Beyond radio-displacement techniques for identification of CB1 ligands: the first application of a fluorescence-quenching assay. *Sci. Rep.* 4(1):3757

43. Veiksina S, Kopanchuk S, Rinken A. 2014. Budded baculoviruses as a tool for a homogeneous fluorescence anisotropy-based assay of ligand binding to G protein-coupled receptors: the case of melanocortin 4 receptors. *Biochim. Biophys. Acta—Biomembr.* 1838(1, Part B):372–81

44. Kral AM, Ozerova N, Close J, Jung J, Chenard M, et al. 2014. Divergent kinetics differentiate the mechanism of action of two HDAC inhibitors. *Biochemistry* 53(4):725–34

45. Göhler A, Büchner C, André S, Doose S, Kaltner H, Gabius H-J. 2011. Sensing ligand binding to a clinically relevant lectin by tryptophan fluorescence anisotropy. *Analyst* 136(24):5270–76

46. Deacon M, Singleton D, Szalkai N, Pasieczny R, Peacock C, et al. 2007. Early evaluation of compound QT prolongation effects: a predictive 384-well fluorescence polarization binding assay for measuring HERG blockade. *J. Pharmacol. Toxicol. Methods* 55(3):238–47

47. Meyners C, Baud MGJ, Fuchter MJ, Meyer-Almes F-J. 2014. Kinetic method for the large-scale analysis of the binding mechanism of histone deacetylase inhibitors. *Anal. Biochem.* 460:39–46

48. Ilien B, Franchet C, Bernard P, Morisset S, Weill CO, et al. 2003. Fluorescence resonance energy transfer to probe human M1 muscarinic receptor structure and drug binding properties. *J. Neurochem.* 85(3):768–78

49. Schiele F, Ayaz P, Fernández-Montalván A. 2015. A universal homogeneous assay for high-throughput determination of binding kinetics. *Anal. Biochem.* 468:42–49

50. Mason JL, Spais C, Husten J, Prouty E, Albom MS, et al. 2012. Comparison of LanthaScreen Eu kinase binding assay and surface plasmon resonance method in elucidating the binding kinetics of focal adhesion kinase inhibitors. *Assay Drug Dev. Technol.* 10(5):468–75

51. Kim B, Tarchevskaya SS, Eggel A, Vogel M, Jardetzky TS. 2012. A time-resolved fluorescence resonance energy transfer assay suitable for high-throughput screening for inhibitors of immunoglobulin E-receptor interactions. *Anal. Biochem.* 431(2):84–89

52. Iwata H, Imamura S, Hori A, Hixon MS, Kimura H, Miki H. 2011. Biochemical characterization of a novel type-II VEGFR2 kinase inhibitor: comparison of binding to non-phosphorylated and phosphorylated VEGFR2. *Bioorg. Med. Chem.* 19(18):5342–51

53. Stoddart LA, Johnstone EKM, Wheal AJ, Goulding J, Robers MB, et al. 2015. Application of BRET to monitor ligand binding to GPCRs. *Nat. Methods* 12(7):661–63

54. Christiansen E, Hudson BD, Hansen AH, Milligan G, Ulven T. 2016. Development and characterization of a potent free fatty acid receptor 1 (FFA1) fluorescent tracer. *J. Med. Chem.* 59(10):4849–58

55. Robers MB, Dart ML, Woodroofe CC, Zimprich CA, Kirkland TA, et al. 2015. Target engagement and drug residence time can be observed in living cells with BRET. *Nat. Commun.* 6:10091

56. Núñez S, Venhorst J, Kruse CG. 2012. Target–drug interactions: first principles and their application to drug discovery. *Drug Discov. Today* 17(1–2):10–22

57. Cooper MA. 2002. Optical biosensors in drug discovery. *Nat. Rev. Drug Discov.* 1(7):515–28

58. Früh V, Ijzerman AP, Siegal G. 2011. How to catch a membrane protein in action: a review of functional membrane protein immobilization strategies and their applications. *Chem. Rev.* 111(2):640–56

59. Huber W. 2005. A new strategy for improved secondary screening and lead optimization using high-resolution SPR characterization of compound-target interactions. *J. Mol. Recognit.* 18(4):273–81

60. Markgren PO, Schaal W, Hamalainen M, Karlen A, Hallberg A, et al. 2002. Relationships between structure and interaction kinetics for HIV-1 protease inhibitors. *J. Med. Chem.* 45(25):5430–39

61. Stenlund P, Frostell-Karlsson Å, Karlsson OP. 2006. Studies of small molecule interactions with protein phosphatases using biosensor technology. *Anal. Biochem.* 353(2):217–25

62. Nordin H, Jungnelius M, Karlsson R, Karlsson OP. 2005. Kinetic studies of small molecule interactions with protein kinases using biosensor technology. *Anal. Biochem.* 340(2):359–68

63. Navratilova I, Dioszegi M, Myszka DG. 2006. Analyzing ligand and small molecule binding activity of solubilized GPCRs using biosensor technology. *Anal. Biochem.* 355(1):132–39

64. Aristotelous T, Ahn S, Shukla AK, Gawron S, Sassano MF, et al. 2013. Discovery of β2 adrenergic receptor ligands using biosensor fragment screening of tagged wild-type receptor. *ACS Med. Chem. Lett.* 4(10):1005–10

65. Rich RL, Errey J, Marshall F, Myszka DG. 2011. Biacore analysis with stabilized G-protein-coupled receptors. *Anal. Biochem.* 409(2):267–72

66. Congreve M, Andrews SP, Doré AS, Hollenstein K, Hurrell E, et al. 2012. Discovery of 1,2,4-triazine derivatives as adenosine A_{2A} antagonists using structure based drug design. *J. Med. Chem.* 55(5):1898–903

67. Bayburt TH, Sligar SG. 2010. Membrane protein assembly into nanodiscs. *FEBS Lett.* 584(9):1721–27

68. Segala E, Errey JC, Fiez-Vandal C, Zhukov A, Cooke RM. 2015. Biosensor-based affinities and binding kinetics of small molecule antagonists to the adenosine A_{2A} receptor reconstituted in HDL like particles. *FEBS Lett.* 589(13):1399–405

69. Bocquet N, Kohler J, Hug MN, Kusznir EA, Rufer AC, et al. 2015. Real-time monitoring of binding events on a thermostabilized human A_{2A} receptor embedded in a lipid bilayer by surface plasmon resonance. *Biochim. Biophys. Acta—Biomembr.* 1848(5):1224–33

70. Gronewold TMA, Baumgartner A, Hierer J, Sierra S, Blind M, et al. 2009. Kinetic binding analysis of aptamers targeting HIV-1 proteins by a combination of a microbalance array and mass spectrometry (MAMS). *J. Proteome Res.* 8(7):3568–77

71. Burnouf D, Ennifar E, Guedich S, Puffer B, Hoffmann G, et al. 2012. KinITC: a new method for obtaining joint thermodynamic and kinetic data by isothermal titration calorimetry. *J. Am. Chem. Soc.* 134(1):559–65

72. Li D, Chen L, Wang R, Liu R, Ge G. 2017. Synergetic determination of thermodynamic and kinetic signatures using isothermal titration calorimetry: a full-curve-fitting approach. *Anal. Chem.* 89(13):7130–38

73. Vauquelin G, Huber W, Swinney DC. 2015. Experimental methods to determine binding kinetics. In *Thermodynamics and Kinetics of Drug Binding*, ed. G Keserü, DC Swinney, pp. 169–89. Weinheim, Ger.: Wiley-VCH

74. Acker MG, Auld DS. 2014. Considerations for the design and reporting of enzyme assays in high-throughput screening applications. *Perspect. Sci.* 1(1):56–73

75. Copeland RA, Basavapathruni A, Moyer M, Scott MP. 2011. Impact of enzyme concentration and residence time on apparent activity recovery in jump dilution analysis. *Anal. Biochem.* 416(2):206–10

76. Callan OH, So OY, Swinney DC. 1996. The kinetic factors that determine the affinity and selectivity for slow binding inhibition of human prostaglandin H synthase 1 and 2 by indomethacin and flurbiprofen. *J. Biol. Chem.* 271(7):3548–54

77. De Vivo M, Masetti M, Bottegoni G, Cavalli A. 2016. Role of molecular dynamics and related methods in drug discovery. *J. Med. Chem.* 59(9):4035–61

78. Basconi JE, Shirts MR. 2013. Effects of temperature control algorithms on transport properties and kinetics in molecular dynamics simulations. *J. Chem. Theory Comput.* 9(7):2887–99

79. Bolhuis PG, Christoph D. 2010. Trajectory-based rare event simulations. In *Reviews in Computational Chemistry*, ed. KB Lipkowitz, pp. 111–210. New York: Wiley

80. Gioia D, Bertazzo M, Recanatini M, Cavalli A. 2017. Dynamic docking: a paradigm shift in computational drug discovery. *Molecules* 22(11):1–21

81. De Vivo M, Cavalli A. 2017. Recent advances in dynamic docking for drug discovery. *WIREs Comput. Mol. Sci.* 7(6):e1320

82. Shan Y, Kim ET, Eastwood MP, Dror RO, Seeliger MA, Shaw DE. 2011. How does a drug molecule find its target binding site? *J. Am. Chem. Soc.* 133(24):9181–83

83. Dror RO, Pan AC, Arlow DH, Borhani DW, Maragakis P, et al. 2011. Pathway and mechanism of drug binding to G-protein-coupled receptors. *PNAS* 108(32):13118–23

84. Decherchi S, Berteotti A, Bottegoni G, Rocchia W, Cavalli A. 2015. The ligand binding mechanism to purine nucleoside phosphorylase elucidated via molecular dynamics and machine learning. *Nat. Commun.* 6:6155

85. Halle B, Persson F. 2013. Analysis of protein dynamics simulations by a stochastic point process approach. *J. Chem. Theory Comput.* 9(6):2838–48

86. Huang D, Caflisch A. 2011. The free energy landscape of small molecule unbinding. *PLOS Comput. Biol.* 7(2):e1002002

87. Pande VS, Beauchamp K, Bowman GR. 2010. Everything you wanted to know about markov state models but were afraid to ask. *Methods* 52(1):99–105

88. Prinz JH, Wu H, Sarich M, Keller B, Senne M, et al. 2011. Markov models of molecular kinetics: generation and validation. *J. Chem. Phys.* 134(17):174105

89. Bowman GR. 2014. An overview and practical guide to building Markov state models. In *An Introduction to Markov State Models and Their Application to Long Timescale Molecular Simulation*, ed. GR Bowman, VS Pande, F Noe, pp. 7–22. Dordrecht, Neth.: Springer

90. Pan AC, Roux B. 2008. Building Markov state models along pathways to determine free energies and rates of transitions. *J. Chem. Phys.* 129(6):64107

91. Guillain F, Thusius D. 1970. Use of proflavine as an indicator in temperature-jump studies of the binding of a competitive inhibitor to trypsin. *J. Am. Chem. Soc.* 92(18):5534–36

92. Buch I, Giorgino T, De Fabritiis G. 2011. Complete reconstruction of an enzyme-inhibitor binding process by molecular dynamics simulations. *PNAS* 108(25):10184–89

93. Plattner N, Noé F. 2015. Protein conformational plasticity and complex ligand-binding kinetics explored by atomistic simulations and Markov models. *Nat. Commun.* 6:7653

94. Doerr S, De Fabritiis G. 2014. On-the-fly learning and sampling of ligand binding by high-throughput molecular simulations. *J. Chem. Theory Comput.* 10(5):2064–69

95. Singhal N, Pande VS. 2005. Error analysis and efficient sampling in Markovian state models for molecular dynamics. *J. Chem. Phys.* 123(20):204909

96. Hinrichs NS, Pande VS. 2007. Calculation of the distribution of eigenvalues and eigenvectors in Markovian state models for molecular dynamics. *J. Chem. Phys.* 126(24):244101

97. Weber JK, Pande VS. 2011. Characterization and rapid sampling of protein folding Markov state model topologies. *J. Chem. Theory Comput.* 7(10):3405–11

98. Cérou F, Guyader A, Lelièvre T, Pommier D. 2011. A multiple replica approach to simulate reactive trajectories. *J. Chem. Phys.* 134(5):54108

99. Teo I, Mayne CG, Schulten K, Lelièvre T. 2016. Adaptive multilevel splitting method for molecular dynamics calculation of benzamidine-trypsin dissociation time. *J. Chem. Theory Comput.* 12(6):2983–89

100. Dickson A, Brooks CL III. 2014. WExplore: hierarchical exploration of high-dimensional spaces using the weighted ensemble algorithm. *J. Phys. Chem. B* 118(13):3532–42

101. Dickson A, Lotz SD. 2016. Ligand release pathways obtained with WExplore: residence times and mechanisms. *J. Phys. Chem. B* 120(24):5377–85

102. Dickson A, Lotz SD. 2017. Multiple ligand unbinding pathways and ligand-induced destabilization revealed by WExplore. *Biophys. J.* 112(4):620–29

103. Lotz SD, Dickson A. 2018. Unbiased molecular dynamics of 11 min timescale drug unbinding reveals transition state stabilizing interactions. *J. Am. Chem. Soc.* 140(2):618–28

104. Dixon T, Lotz SD, Dickson A. 2018. Predicting ligand binding affinity using on- and off-rates for the SAMPL6 SAMPLing challenge. *J. Comput. Aided. Mol. Des.* 32(10):1001–12

105. Zhou H-X. 2010. Rate theories for biologists. *Q. Rev. Biophys.* 43(2):219–93

106. Ermak DL, McCammon JA. 1978. Brownian dynamics with hydrodynamic interactions. *J. Chem. Phys.* 69(4):1352–60

107. Decherchi S, Masetti M, Vyalov I, Rocchia W. 2015. Implicit solvent methods for free energy estimation. *Eur. J. Med. Chem.* 91:27–42

108. Sung JC, Van Wynsberghe AW, Amaro RE, Li WW, McCammon JA. 2010. Role of secondary sialic acid binding sites in influenza N1 neuraminidase. *J. Am. Chem. Soc.* 132(9):2883–85

109. Northrup SH, Allison SA, McCammon JA. 1984. Brownian dynamics simulation of diffusion-influenced bimolecular reactions. *J. Chem. Phys.* 80(4):1517–24

110. Vijaykumar A, Bolhuis PG, ten Wolde PR. 2016. The intrinsic rate constants in diffusion-influenced reactions. *Faraday Discuss.* 195:421–41

111. Smoluchowski MV. 1916. Drei Vortrage uber Diffusion, Brownsche Bewegung und Koagulation von Kolloidteilchen. *Phys. Z.* 17:557–85

112. Steinhauser MO. 2008. *Multiscale Modeling of Fluids and Solids: Theory and Applications*. Berlin: Springer-Verlag

113. Amaro RE, Mulholland AJ. 2018. Multiscale methods in drug design bridge chemical and biological complexity in the search for cures. *Nat. Rev. Chem.* 2:148

114. Votapka LW, Amaro RE. 2015. Multiscale estimation of binding kinetics using Brownian dynamics, molecular dynamics and milestoning. *PLOS Comput. Biol.* 11(10):e1004381

115. Masetti M, Berti C, Ocello R, Di Martino GP, Recanatini M, et al. 2016. Multiscale simulations of a two-pore potassium channel. *J. Chem. Theory Comput.* 12(12):5681–87

116. Zeller F, Luitz MP, Bomblies R, Zacharias M. 2017. Multiscale simulation of receptor-drug association kinetics: application to neuraminidase inhibitors. *J. Chem. Theory Comput.* 13(10):5097–105

117. Votapka LW, Jagger BR, Heyneman AL, Amaro RE. 2017. SEEKR: simulation enabled estimation of kinetic rates, a computational tool to estimate molecular kinetics and its application to trypsin-benzamidine binding. *J. Phys. Chem. B* 121(15):3597–606

118. Vanden-Eijnden E, Venturoli M, Ciccotti G, Elber R. 2008. On the assumptions underlying milestoning. *J. Chem. Phys.* 129(17):174102

119. Faradjian AK, Elber R. 2004. Computing time scales from reaction coordinates by milestoning. *J. Chem. Phys.* 120(23):10880–89

120. Jagger BR, Lee CT, Amaro RE. 2018. Quantitative ranking of ligand binding kinetics with a multiscale milestoning simulation approach. *J. Phys. Chem. Lett.* 9(17):4941–48

121. Haldar S, Comitani F, Saladino G, Woods C, van der Kamp MW, et al. 2018. A multiscale simulation approach to modeling drug-protein binding kinetics. *J. Chem. Theory Comput.* 14(11):6093–101

122. Juraszek J, Saladino G, van Erp TS, Gervasio FL. 2013. Efficient numerical reconstruction of protein folding kinetics with partial path sampling and pathlike variables. *Phys. Rev. Lett.* 110(10):108106

123. Woods CJ, Manby FR, Mulholland AJ. 2008. An efficient method for the calculation of quantum mechanics/molecular mechanics free energies. *J. Chem. Phys.* 128(1):14109

124. Masetti M, Rocchia W. 2014. Molecular mechanics and dynamics: numerical tools to sample the configuration space. *Front. Biosci.* 19:578–604

125. Abrams C, Bussi G. 2013. Enhanced sampling in molecular dynamics using metadynamics, replica-exchange, and temperature-acceleration. *Entropy* 16(1):163–99

126. Bui JM, Henchman RH, McCammon JA. 2003. The dynamics of ligand barrier crossing inside the acetyl-cholinesterase gorge. *Biophys. J.* 85(4):2267–72

127. Torrie GM, Valleau JP. 1977. Nonphysical sampling distributions in Monte Carlo free-energy estimation: umbrella sampling. *J. Comput. Phys.* 23(2):187–99

128. Northrup SH, Pear MR, Lee CY, McCammon JA, Karplus M. 1982. Dynamical theory of activated processes in globular proteins. *PNAS* 79(13):4035–39

129. Allnér O, Nilsson L, Villa A. 2012. Magnesium ion-water coordination and exchange in biomolecular simulations. *J. Chem. Theory Comput.* 8(4):1493–502

130. Masetti M, Musiani F, Bernetti M, Falchi F, Cavalli A, et al. 2017. Development of a multisite model for Ni(II) ion in solution from thermodynamic and kinetic data. *J. Comput. Chem.* 38(21):1834–43

131. Marinelli F, Pietrucci F, Laio A, Piana S. 2009. A kinetic model of Trp-cage folding from multiple biased molecular dynamics simulations. *PLOS Comput. Biol.* 5(8):e1000452

132. Voter AF. 2007. Introduction to the kinetic Monte Carlo method. In *Radiation Effects in Solids*, ed. KE Sickafus, EA Kotomin, BP Uberuaga, pp. 1–23. Dordrecht, Neth.: Springer

133. Bortz AB, Kalos MH, Lebowitz JL. 1975. A new algorithm for Monte Carlo simulation of Ising spin systems. *J. Comput. Phys.* 17(1):10–18

134. Pietrucci F, Marinelli F, Carloni P, Laio A. 2009. Substrate binding mechanism of HIV-1 protease from explicit-solvent atomistic simulations. *J. Am. Chem. Soc.* 131(33):11811–18

135. Piana S, Laio A. 2007. A bias-exchange approach to protein folding. *J. Phys. Chem. B* 111(17):4553–59

136. Branduardi D, Gervasio FL, Parrinello M. 2007. From A to B in free energy space. *J. Chem. Phys.* 126(5):54103

137. Dellago C, Bolhuis PG. 2004. Activation energies from transition path sampling simulations. *Mol. Simul.* 30(11–12):795–99

138. Morando MA, Saladino G, D'Amelio N, Pucheta-Martinez E, Lovera S, et al. 2016. Conformational selection and induced fit mechanisms in the binding of an anticancer drug to the C-Src kinase. *Sci. Rep.* 6:24439

139. Tiwary P, Parrinello M. 2013. From metadynamics to dynamics. *Phys. Rev. Lett.* 111(23):230602

140. Tiwary P, Limongelli V, Salvalaglio M, Parrinello M. 2015. Kinetics of protein-ligand unbinding: predicting pathways, rates, and rate-limiting steps. *PNAS* 112(5):E386–91

141. Casasnovas R, Limongelli V, Tiwary P, Carloni P, Parrinello M. 2017. Unbinding kinetics of a P38 MAP kinase type II inhibitor from metadynamics simulations. *J. Am. Chem. Soc.* 139(13):4780–88

142. Callegari D, Lodola A, Pala D, Rivara S, Mor M, et al. 2017. Metadynamics simulations distinguish short-and long-residence-time inhibitors of cyclin-dependent kinase 8. *J. Chem. Inf. Model.* 57(2):159–69

143. Mollica L, Decherchi S, Zia SR, Gaspari R, Cavalli A, Rocchia W. 2015. Kinetics of protein-ligand unbinding via smoothed potential molecular dynamics simulations. *Sci. Rep.* 5:11539

144. Mark AE, van Gunsteren WF, Berendsen HJC. 1991. Calculation of relative free energy via indirect pathways. *J. Chem. Phys.* 94(5):3808–16

145. Sinko W, Miao Y, de Oliveira CAF, McCammon JA. 2013. Population based reweighting of scaled molecular dynamics. *J. Phys. Chem. B* 117(42):12759–68

146. Tsujishita H, Moriguchi I, Hirono S. 1993. Potential-scaled molecular dynamics and potential annealing: effective conformational search techniques for biomolecules. *J. Phys. Chem.* 97(17):4416–20

147. Mollica L, Theret I, Antoine M, Perron-Sierra F, Charton Y, et al. 2016. Molecular dynamics simulations and kinetic measurements to estimate and predict protein-ligand residence times. *J. Med. Chem.* 59(15):7167–76

148. Decherchi S, Bottegoni G, Spitaleri A, Rocchia W, Cavalli A. 2018. BiKi life sciences: a new suite for molecular dynamics and related methods in drug discovery. *J. Chem. Inf. Model.* 58(2):219–24

149. Lüdemann SK, Lounnas V, Wade RC. 2000. How do substrates enter and products exit the buried active site of cytochrome P450cam? 1. Random expulsion molecular dynamics investigation of ligand access channels and mechanisms. *J. Mol. Biol.* 303(5):797–811

150. Kokh DB, Amaral M, Bomke J, Grädler U, Musil D, et al. 2018. Estimation of drug-target residence times by τ-random acceleration molecular dynamics simulations. *J. Chem. Theory Comput.* 14(7):3859–69